ELSEVIER

Real light emitter in the bioluminescence of the calcium-activated photoproteins aequorin and obelin: light emission from the singlet-excited state of coelenteramide phenolate anion in a contact ion pair

Kotaro Mori,[a] Shojiro Maki,[a] Haruki Niwa,[a] Hiroshi Ikeda[b] and Takashi Hirano[a,*]

[a]Department of Applied Physics and Chemistry, The University of Electro-Communications, Chofu, Tokyo 182-8585, Japan
[b]Department of Chemistry, Graduate School of Science, Tohoku University, Sendai 980-8578, Japan

Abstract—Fluorescence of the phenolate anion ($3(O)^-$) and the amide anion ($5(N)^-$) of coelenteramide analogues in ion pairs with various counter cations was systematically investigated to elucidate the ionic structure of the light emitter in the bioluminescence of the calcium-activated photoproteins aequorin and obelin. The fluorescent properties of $3(O)^-$ in an ion pair with a conjugate acid of an organic base ($BASE-H^+$) were varied depending on the structural variation of the ion pair and the solvent polarity. In particular, the fluorescence of $3(O)^-$ in the ion pair with the conjugate acid of n-butylamine ($NBA-H^+$) indicates that the singlet-excited state of $3(O)^-$ ($^13(O)^{-*}$) and $NBA-H^+$ make a contact ion pair in which the fluorescence emission maxima of $3(O)^-$ is sensitive to the solvent polarity and the fluorescence quantum yields of $3(O)^-$ increase in a less polar solvent. The results also confirm that $^13(O)^{-*}$ is a twisted intramolecular charge transfer state. By contrast, the fluorescence of $5(N)^-$ in an ion pair depends little on the $BASE-H^+$ or the solvent polarity. Based on these results, we conclude that the light emitter in aequorin and obelin bioluminescences is the singlet-excited state of coelenteramide phenolate anion $2(O)^-$ ($^12(O)^{-*}$) in a contact ion pair with an imidazolium side chain of a histidine residue, which is located at the less polar active sites of the photoproteins. We also propose a mechanism for the bioluminescence reaction, including the chemiexcitation process to give $^12(O)^{-*}$.
© 2006 Elsevier Ltd. All rights reserved.

1. Introduction

Calcium-activated photoproteins are light-generating molecules for several marine bioluminescent organisms.[1] The biochemical aspects of the photoproteins aequorin[2,3] and obelin,[4] isolated from the jellyfish *Aequorea* and *Obelia*, respectively, have been particularly well investigated. Chemical study on calcium-activated photoproteins was pioneered by Shimomura et al., who discovered aequorin.[2a] Aequorin is made from apoaequorin (apoprotein), coelenterazine (**1**) (substrate), and molecular oxygen (O_2). Chelation of Ca^{2+} with the EF-hands of aequorin initiates the bioluminescence reaction, which gives a fluorescent protein (FLP),[5] CO_2, and bluish light (Scheme 1). The crystal structure of aequorin helped to clarify its supramolecular structure, containing oxygenated coelenterazine in the active site.[6] Recent research on the crystal structures of the various forms of

obelin has also yielded important information on the character of obelin's active site.[7]
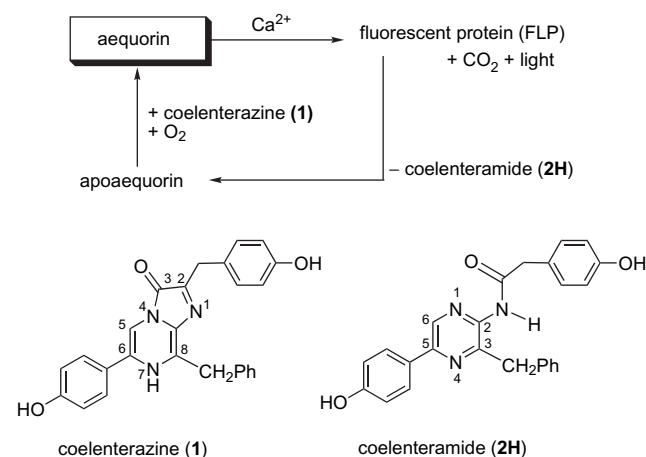
Scheme 1.

The bioluminescence reaction of the calcium-activated photoproteins is based on the reaction of **1** with O_2, which

yields coelenteramide (**2H**), CO_2, and light.[8–10] Light emission occurs from the singlet-excited state of the anion species of **2H** ($^1\textbf{2}^{-*}$) in apoprotein, to give FLP, a complex of **2H** and apoprotein.[11] The structure elucidation of $^1\textbf{2}^{-*}$ in apoprotein is one of the controversies in the reaction mechanism. Two structures are possible for $^1\textbf{2}^{-*}$: the singlet-excited state of an amide anion **2(N)**$^-$ ($^1\textbf{2(N)}^{-*}$) and the singlet-excited state of a phenolate anion **2(O)**$^-$ ($^1\textbf{2(O)}^{-*}$) (Scheme 2). Both anions have an anionic center conjugating with the fluorescent core, the pyrazine ring.
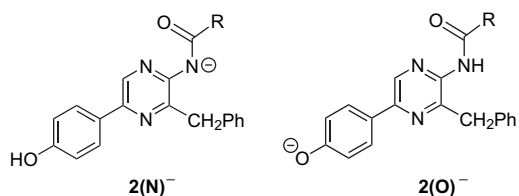

Scheme 2. R=(4-hydroxyphenyl)methyl or (4-oxidophenyl)methyl.

Excited amide anion $^1\textbf{2(N)}^{-*}$ is the light emitter of a chemiluminescence reaction of **1** in an aprotic solvent such as *N,N*-dimethylformamide (DMF) and dimethylsulfoxide (DMSO).[12,13] Because the emission wavelengths of the chemiluminescence of **1** and the bioluminescence of aequorin are similar to each other, $^1\textbf{2(N)}^{-*}$ has been believed as the light emitter in aequorin bioluminescence.[12–14] However, we noticed that this explanation cannot account for the fact that the fluorescence emission of FLP obtained from aequorin occurs from common $^1\textbf{2}^{-*}$ to the light emission in aequorin bioluminescence.[11a,15] Thus, we are the first to propose that $^1\textbf{2(O)}^{-*}$ is the light emitter in aequorin bioluminescence.[15–17] The fact suggests the generation of $^1\textbf{2(O)}^{-*}$ in aequorin bioluminescence, because it is conceivable that **2H** eliminates a proton from the phenolic hydroxy group with a moderate acidity[18] rather than from the amide moiety with a weak acidity.[19–21] In addition, we found that **2(O)**$^-$ in benzene showed the fluorescence spectrum similar to the emission spectrum of aequorin bioluminescence,[17] supporting that the light emitter is $^1\textbf{2(O)}^{-*}$ in apoaequorin, whose active site has a polarity similar to benzene.

The mechanism involving a light emission from $^1\textbf{2(O)}^{-*}$ in aequorin is now applied to obelin bioluminescence.[7b,22] There is confusion in some reports, where $^1\textbf{2(O)}^{-*}$ in polar and in less polar solvents has been categorized as a 'quinoid anion' and an 'ion pair,' respectively.[7b,22,23] However, the quinoid form, shown in Scheme 3c, is only one of the several resonance structures of $^1\textbf{2(O)}^{-*}$. Similarly, we should not distinguish $^1\textbf{2(O)}^{-*}$ in a less polar solvent as an ion pair, because $^1\textbf{2(O)}^{-*}$ is only a component of the ion pair. To precisely understand the fundamental characteristics of $^1\textbf{2(O)}^{-*}$, we have to further establish the spectroscopic

properties of **2(O)**$^-$ in a chemically defined molecular environment, such as an ion pair with a counter cation.

In the previous study we reported the florescence of **3a(O)**$^-$, an analogue of **2(O)**$^-$ having an octanoyl group for improving solubility in various solvents, though we did not clarify the influence of an ion pair of $^1\textbf{3a(O)}^{-*}$ with a counter cation on its fluorescence.[17b] To confirm the mechanism for light emission from $^1\textbf{2(O)}^{-*}$ in the photoprotein, here we reinvestigate the florescence of **3a(O)**$^-$ in ion pairs with conjugate acids of several organic bases as counter cations. The fluorescence of methyl analogue **3b(O)**$^-$ in an ion pair was also investigated to clarify steric effects of the methyl group at C6 on the π-conjugation between the pyrazine ring and the 4-oxidophenyl (4-O$^-$C$_6$H$_4$) group.[24] Furthermore, we investigated fluorescence emission from $^1\textbf{5(N)}^{-*}$ in an ion pair generated by chemiluminescence reactions of coelenterazine analogue **4** in various solvents. Herein we report the spectroscopic characteristics of **3H** and those of **3(O)**$^-$ and **5(N)**$^-$ in an ion pair with a counter cation. We show that the fluorescence of **3(O)**$^-$ depends on a structural variation of an ion pair, while that of **5(N)**$^-$ does not. We also reconfirm that $^1\textbf{2(O)}^{-*}$ is the light emitter in the bioluminescence of aequorin and obelin, and we propose a bioluminescence reaction mechanism involving a chemiexcitation process to give $^1\textbf{2(O)}^{-*}$.

3aH: R = H
3bH: R = CH$_3$

3a(O)$^-$: R = H
3b(O)$^-$: R = CH$_3$

4

5H: R = H
**5(N)**$^-$: R = $\ominus$
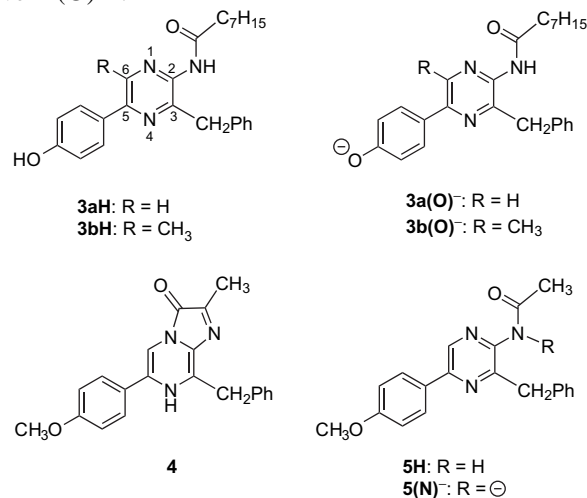
2. Results and discussion

2.1. UV–vis absorption spectra of coelenteramide analogue 3H in the presence of organic bases

Coelenteramide analogue **3aH** was prepared by the procedure previously reported.[17b] Analogue **3bH** was prepared
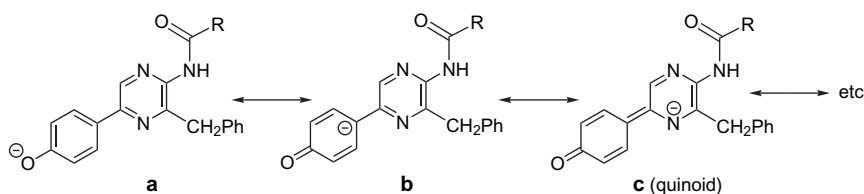
Scheme 3. R=(4-hydroxyphenyl)methyl or (4-oxidophenyl)methyl.

from 6-methylpyrazinamine by the procedure shown in Scheme 4. Pyrazinamine precursor 3-benzyl-5-(4-benzyloxy-phenyl)-6-methylpyrazinamine was prepared by bromination of 6-methylpyrazinamine with tetrabutylammonium tribromide followed by selective Stille and Suzuki couplings. Acylation of the pyrazinamine precursor and the following hydrogenolysis gave **3bH**.
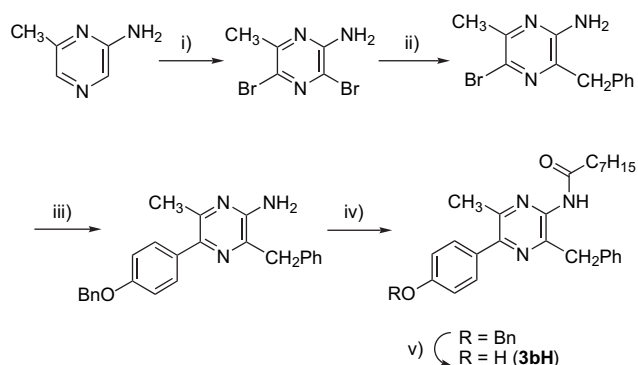
Scheme 4. Reagent and conditions: (i) $(C_4H_9)_4NBr_3$, pyridine, $CHCl_3$, reflux, 46%; (ii) $Bn(C_4H_9)_3Sn$, $PdCl_2(PPh_3)_2$, DMF, 130 °C, 36%; (iii) $BnOC_6H_4B(OH)_2$, $Pd(PPh_3)_4$, 1,4-dioxane, 2 mol L^{-1} Na_2CO_3 aq, 110 °C, 94%; (iv) $C_7H_{15}COCl$, pyridine, CH_2Cl_2, 0 °C, 52%; (v) H_2, Pd–C, $C_2H_5OH/CH_3CO_2C_2H_5$, 67%.

UV–vis absorption spectra of **3H** were measured in *p*-xylene, toluene, benzene, benzene/chloroform (20:1), chloro-benzene, 1-chloropropane, benzene/chloroform (2:1), 1,2-dichlorobenzene, chloroform, dichloromethane, 1,2-dichloroethane, benzonitrile, *N,N*-dimethylacetamide (DMAc), DMF, propionitrile, DMSO, and acetonitrile in the absence and presence of an organic base. In this study, *n*-butylamine (NBA), 1,1,3,3-tetramethylguanidine (TMG), and 1,8-diaza-bicyclo[5.4.0]undec-7-ene (DBU) were used as an organic base (BASE). Thus, their conjugate acids (BASE–H$^+$) will become a counter cation for **3(O)**$^-$ in an ion pair. Selected spectra are shown in Figure 1 and the spectral data are summarized in Tables 1 and 2, where the data are listed in order of the solvent polarity scale $E_T(30)$ (in kcal mol^{-1}).[25]

As reported previously,[17b] two types of characteristic spectral changes of the lowest energy band of **3H** were observed in the presence of BASE. One is type I, which caused the small shift ($\Delta\lambda < 12$ nm) in a less polar solvent. Type II is the other, causing a large bathochromic shift ($\Delta\lambda > 20$ nm) in a more polar solvent. Type I and II spectral changes were caused by the formation of a 1:1 hydrogen-bonded complex of **3H** and BASE ([BASE···**3H**]) and the formation of an ion pair of **3(O)**$^-$ with BASE–H$^+$ ([BASE–H$^+$/**3(O)**$^-$]), respectively (Scheme 5).
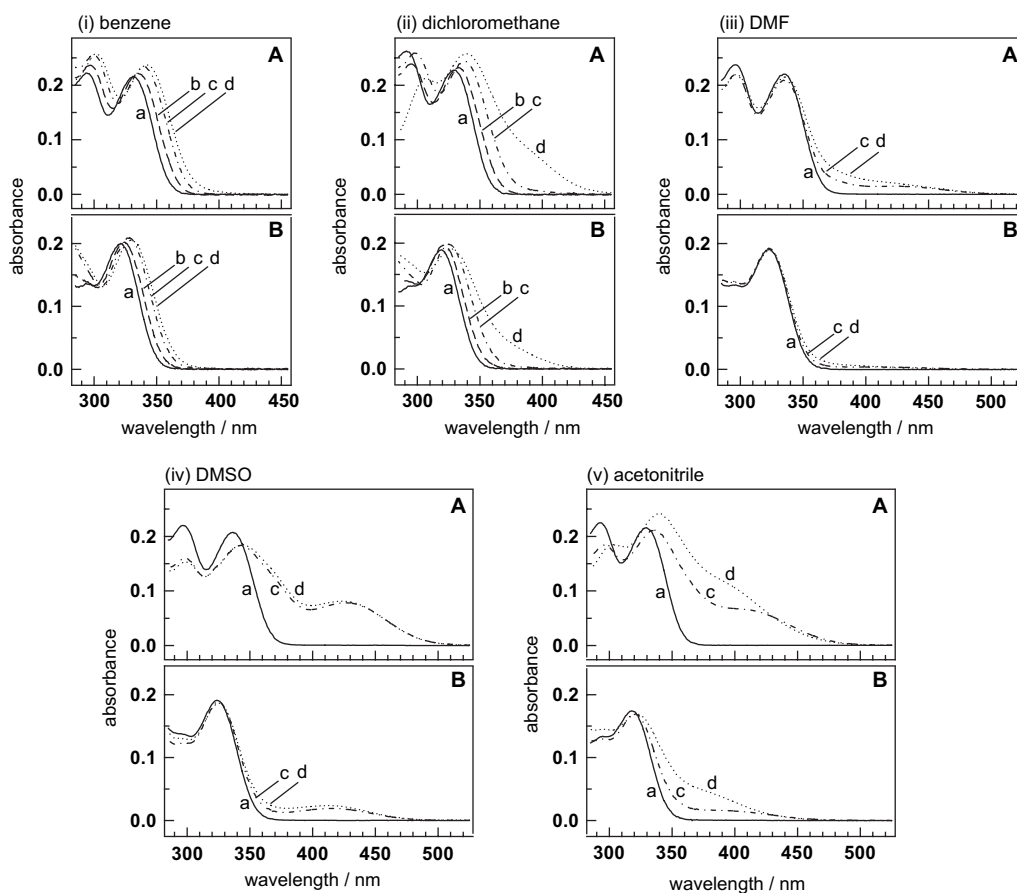
Figure 1. UV–vis absorption spectra of **3aH** (A, 1.5×10^{-5} mol L^{-1}) and **3bH** (B, 1.5×10^{-5} mol L^{-1}) in selected solvents in the absence and presence of organic bases (1.0×10^{-2} mol L^{-1}) at 25 °C; organic base: none (a), NBA (b), TMG (c), and DBU (d). The selected solvents are benzene (i), dichloromethane (ii), DMF (iii), DMSO (iv), and acetonitrile (v).

Table 1. UV–vis absorption data of **3aH** (1.5×10^{-5} mol L^{-1}) in various solvents in the absence and presence of organic bases (NBA, TMG, and DBU) at 25 °C

Solvent	$E_T(30)$/kcal mol^{-1}	λ_{max}/nm ($\varepsilon/10^4$)[a]	λ_{max}/nm (absorbance)		
		3aH	**3aH+NBA**[b]	**3aH+TMG**[b]	**3aH+DBU**[b]
p-Xylene	33.1	332 (1.05)	335 (0.164)	340 (0.170) 300 (0.176)	342 (0.188) 302 (0.198)
Toluene	33.9	332 (1.24)	335 (0.212)	340 (0.228)	342 (0.222) 302 (0.242)
Benzene	34.3	331 (1.44) 294 (1.48)	335 (0.224) 297 (0.237)	340 (0.233) 299 (0.255)	343 (0.237) 301 (0.258)
Benzene/chloroform (20:1)	36.4	331 (1.46) 295 (1.50)	335 (0.228) 297 (0.242)	340 (0.239) 300 (0.257)	342 (0.242) 302 (0.261)
Chlorobenzene	36.8	331 (1.16) 291 (1.28)	336 (0.186) 298 (0.200)	340 (0.212) 300 (0.239)	343 (0.218) 304 (0.233)
1-Chloropropane	37.4	329 (1.16) 293 (1.22)	332 (0.185) 295 (0.203)	339 (0.212) 299 (0.237)	340 (0.221) 301 (0.249)
Benzene/chloroform (2:1)	38.0	331 (1.49) 294 (1.56)	334 (0.221) 296 (0.230)	338 (0.228) 299 (0.243)	390 (0.035, sh) 340 (0.228) 302 (0.261)
1,2-Dichlorobenzene	38.0	332 (1.14)	339 (0.176)	342 (0.198) 302 (0.221)	343 (0.222) 304 (0.249)
Chloroform	39.1	331 (1.33) 294 (1.33)	333 (0.231) 295 (0.237)	338 (0.234) 298 (0.246)	380 (0.072, sh) 331 (0.227) 302 (0.212)
Dichloromethane	40.7	330 (1.52) 291 (1.75)	333 (0.233) 295 (0.239)	338 (0.245) 298 (0.258)	380 (0.102, sh) 339 (0.258) 307 (0.213)
1,2-Dichloroethane	41.3	331 (1.43) 293 (1.45)	334 (0.219) 295 (0.224)	390 (0.014, sh) 338 (0.227) 299 (0.242)	375 (0.047, sh) 338 (0.227) 303 (0.227)
Benzonitrile	41.5	334 (1.36)	337 (0.204)	400 (0.010, sh) 338 (0.207)	390 (0.063, sh) 341 (0.219)
DMAc	42.9	335 (1.54) 296 (1.83)	—[c]	336 (0.222) 298 (0.248)	400 (0.010, sh) 337 (0.224) 297 (0.276)
DMF	43.2	336 (1.47) 296 (1.58)	—[c]	430 (0.014, sh) 335 (0.209) 296 (0.219)	410 (0.024, sh) 335 (0.215) 297 (0.221)
Propionitrile	43.6	330 (1.46) 292 (1.56) 274 (1.52)	334 (0.224) 296 (0.246) 278 (0.224)	385 (0.023, sh) 333 (0.227) 296 (0.233) 276 (0.210)	385 (0.084, sh) 337 (0.243) 299 (0.218)
DMSO	45.1	337 (1.38) 297 (1.47)	—[c]	426 (0.078) 343 (0.183) 299 (0.159)	423 (0.081) 344 (0.186) 299 (0.153)
Acetonitrile	45.6	327 (1.44) 293 (1.50) 272 (1.47)	—[c]	410 (0.066, sh) 336 (0.212) 296 (0.185) 273 (0.177)	400 (0.105, sh) 339 (0.242) 302 (0.185)

[a] Extinction coefficient in L mol^{-1} cm^{-1}.
[b] Concentrations of the organic bases were 1.0×10^{-2} mol L^{-1}.
[c] Absorption spectra of **3aH** did not change in the presence of NBA.

The type I spectral change of **3H** was observed in the presence of BASE in solvents from *p*-xylene (top) to benzonitrile and propionitrile, listed in Tables 1 and 2. In the presence of DBU in benzene/chloroform (2:1), 1,2-dichlorobenzene, chloroform, dichloromethane, 1,2-dichloroethane, benzonitrile, and propionitrile, both the type I and II spectral changes were observed. Typical spectra are shown in Figure 1i and ii. Formation of [BASE···**3H**] was mainly observed in the solvents with low ionizing power. A partial generation of [DBU–H$^+$/**3(O)**$^-$] in these solvents was also observed, because DBU has high enough basicity to eliminate a proton from the phenolic hydroxy groups of **3H**. The order of $\Delta\lambda$, DBU>TMG>NBA, corresponds to the reported acidities (pK_a) of their conjugated acids, 24.1, 23.3, and 18.1, respectively, in acetonitrile.[26] The order of $\Delta\lambda$ also corresponds to the formation constants (K, Scheme 5) of [DBU···**3aH**], [TMG···**3aH**], and [NBA···**3aH**]: 7800,

1430, and 220[17b] mol^{-1} L, respectively, in benzene at 25 °C. Therefore, the more basic an organic base becomes, the stronger **3H** makes a hydrogen bond with the organic base and the more $\Delta\lambda$ and K increase.

The type II spectral changes for **3H** were observed in the presence of TMG and DBU in DMAc, DMF, DMSO, and acetonitrile, while the addition of NBA did not affect the original spectra of **3H** (Fig. 1iii–v). These solvents have enough ionizing power to generate [BASE–H$^+$/**3(O)**$^-$]. In addition, TMG and DBU have high enough basicities to generate **3(O)**$^-$ from **3H**, but NBA does not. Absorption spectra of [TMG–H$^+$/**3(O)**$^-$] and [DBU–H$^+$/**3(O)**$^-$] were similar to each other, suggesting that the interaction of **3(O)**$^-$ with TMG–H$^+$ in the ion pair is similar to that of DBU–H$^+$. One of the characteristics of the spectral changes is that a growth of the absorption of [TMG–H$^+$/**3b(O)**$^-$] or [DBU–H$^+$/**3b(O)**$^-$]

Table 2. UV–vis absorption data of **3bH** (1.5×10^{-5} mol L^{-1}) in various solvents in the absence and presence of organic bases (NBA, TMG, and DBU) at 25 °C

Solvent	$E_T(30)$/kcal mol^{-1}	λ_{max}/nm ($\varepsilon/10^4$)[a]	λ_{max}/nm (absorbance)		
		3bH	**3bH+NBA**[b]	**3bH+TMG**[b]	**3bH+DBU**[b]
p-Xylene	33.1	323 (1.35)	324 (0.201)	329 (0.206)	331 (0.207)
Toluene	33.9	322 (1.32)	324 (0.203)	328 (0.209)	329 (0.209)
Benzene	34.3	321 (1.33)	324 (0.203)	328 (0.210)	330 (0.206)
Benzene/chloroform (20:1)	36.4	321 (1.32)	323 (0.201)	327 (0.198)	329 (0.204)
Chlorobenzene	36.8	322 (1.43)	325 (0.218)	330 (0.225)	331 (0.225)
1-Chloropropane	37.4	320 (1.38)	322 (0.207)	327 (0.210)	328 (0.213)
				275 (0.206)	277 (0.216)
Benzene/chloroform (2:1)	38.0	321 (1.30)	324 (0.198)	327 (0.198)	380 (0.017, sh)
					331 (0.192)
1,2-Dichlorobenzene	38.0	321 (1.31)	325 (0.209)	330 (0.216)	331 (0.215)
Chloroform	39.1	319 (1.28)	322 (0.195)	326 (0.194)	370 (0.038, sh)
					322 (0.180)
Dichloromethane	40.7	319 (1.26)	321 (0.197)	325 (0.198)	370 (0.048, sh)
				274 (0.192)	328 (0.191)
					275 (0.192)
1,2-Dichloroethane	41.3	320 (1.31)	322 (0.197)	327 (0.203)	326 (0.192)
				273 (0.200)	276 (0.186)
Benzonitrile	41.5	323 (1.21)	325 (0.183)	390 (0.007, sh)	385 (0.029, sh)
				325 (0.183)	329 (0.185)
DMAc	42.9	323 (1.39)	—[c]	326 (0.197)	324 (0.198)
DMF	43.2	323 (1.27)	—[c]	410 (0.004, sh)	400 (0.005, sh)
		294 (0.89)		333 (0.192)	333 (0.189)
				294 (0.140)	295 (0.140)
Propionitrile	43.6	320 (1.24)	321 (0.188)	380 (0.008, sh)	375 (0.037, sh)
				321 (0.188)	323 (0.186)
DMSO	45.1	324 (1.27)	—[c]	416 (0.020)	412 (0.024)
				326 (0.188)	325 (0.186)
Acetonitrile	45.6	318 (1.16)	—[c]	390 (0.016, sh)	380 (0.045, sh)
		295 (0.89)		321 (0.170)	322 (0.170)
		263 (1.10)		294 (0.129)	271 (0.165)
				265 (0.156)	

[a] Extinction coefficient in L mol^{-1} cm^{-1}.
[b] Concentrations of the organic bases were 1.0×10^{-2} mol L^{-1}.
[c] Absorption spectra of **3bH** did not change in the presence of NBA.

was smaller than that of [TMG–H$^+$/**3a(O)**$^-$] or [DBU–H$^+$/**3a(O)**$^-$]. The K value for the formation of [TMG–H$^+$/**3b(O)**$^-$] in DMSO, 28 mol^{-1} L at 25 °C, is much smaller than that of [TMG–H$^+$/**3a(O)**$^-$], 480 mol^{-1} L at 25 °C,[17b] clearly indicating that the generation of **3b(O)**$^-$ from **3bH**

is less favorable than that of **3a(O)**$^-$ from **3aH**. This is explained by the methyl group at C6 in **3b(O)**$^-$ sterically inhibiting the π-electronic conjugation between the 4-oxido-phenyl and amidopyrazine moieties (vide infra) to decrease the molecular stability.

Scheme 5.

3b(O)⁻
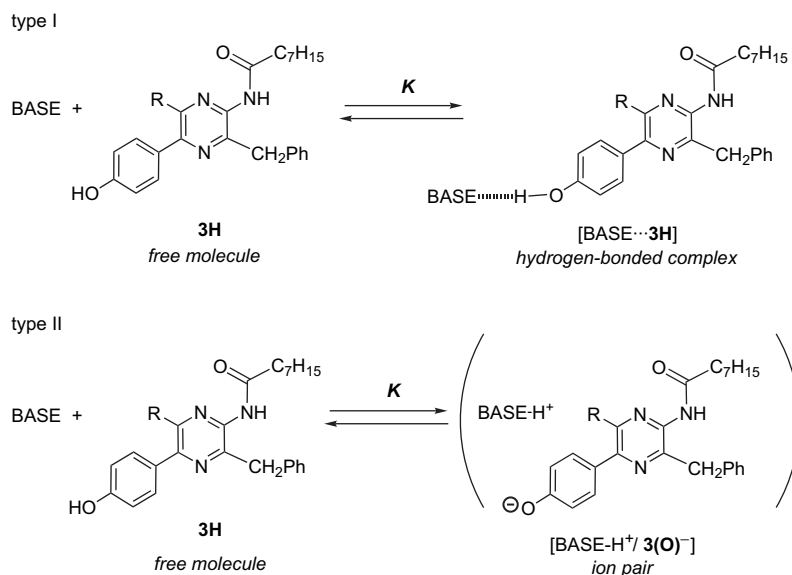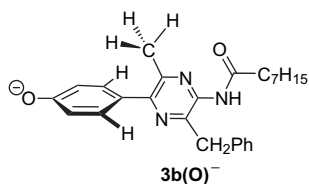
2.2. Fluorescent properties of phenolate anions 3(O)⁻ in ion pairs with conjugate acids of organic bases

Growth of the fluorescence emission band of $3(O)^-$ was observed along with decreasing fluorescence intensity of the neutral molecule $3H$ in the presence of NBA,[17b] TMG,[17b] and DBU, as shown in the selected spectra (Fig. 2). We also confirmed that fluorescence excitation spectra of $3(O)^-$ in the presence of organic bases correspond to their absorption spectra. Corresponding to the type I and II spectral changes in the UV–vis absorption, there are two possible processes to generate $^1 3(O)^{-*}$ in an ion pair with a BASE–H⁺ (Scheme 6).[17] One is a stepwise process via [BASE···$^1 3H^*$] generated by electronic excitation of [BASE···$3H$], as shown in Scheme 6a. The other is a direct electronic excitation process from [BASE–H⁺/$3(O)^-$] (Scheme 6b). Both processes show the fluorescence from [BASE–H⁺/$^1 3(O)^{-*}$].

Fluorescence emission maxima (λ_{FL}) and quantum yields (Φ_f) are summarized in Tables 3 and 4. The Φ_f values of [BASE–H⁺/$3(O)^-$] were obtained by subtracting the fluorescences of $3H$ from the total spectra. Because the

fluorescence emission from $^1 3(O)^{-*}$ in an ion pair has an intramolecular charge transfer (ICT) nature, energies E_{FL} (in kcal mol⁻¹) calculated from the λ_{FL} of [BASE–H⁺/$3(O)^-$] show a linear correlation to $E_T(30)$.[17b] Thus, we made E_{FL}–$E_T(30)$ plots of $3(O)^-$ in the ion pairs with NBA–H⁺, TMG–H⁺, and DBU–H⁺, as shown in Figure 3. The E_{FL}–$E_T(30)$ correlations were $E_{FL}=-1.04E_T(30)+97$ ($r=-0.96$), $E_{FL}=-0.89E_T(30)+88$ ($r=-0.98$), and $E_{FL}=-0.90E_T(30)+89$ ($r=-0.98$), for [NBA–H⁺/$3a(O)^-$], [TMG–H⁺/$3a(O)^-$], and [DBU–H⁺/$3a(O)^-$], respectively.[27] Similarly, $E_{FL}=-1.40E_T(30)+111$ ($r=-0.99$), $E_{FL}=-1.00E_T(30)+92$ ($r=-0.97$), and $E_{FL}=-1.02E_T(30)+93$ ($r=-0.98$) were for [NBA–H⁺/$3b(O)^-$], [TMG–H⁺/$3b(O)^-$], and [DBU–H⁺/$3b(O)^-$], respectively.

The E_{FL}–$E_T(30)$ correlations for [TMG–H⁺/$3(O)^-$] and [DBU–H⁺/$3(O)^-$] were similar to each other, while the slopes and intercepts of the linear E_{FL}–$E_T(30)$ correlations for [NBA–H⁺/$3(O)^-$] were larger than those for [TMG–H⁺/$3(O)^-$] or [DBU–H⁺/$3(O)^-$]. Similarly, the Φ_f of [TMG–H⁺/$3(O)^-$] and [DBU–H⁺/$3(O)^-$] were similar to each other, while most of the Φ_f of [NBA–H⁺/$3(O)^-$] were larger than those of [TMG–H⁺/$3(O)^-$] or [DBU–H⁺/$3(O)^-$]. These results indicate that there are two modes of interaction between $^1 3(O)^{-*}$ and a BASE–H⁺, which may be caused by a structural variation of an ion pair: a solvent separated ion pair (SSIP) for [TMG–H⁺/$^1 3(O)^{-*}$] or [DBU–H⁺/$^1 3(O)^{-*}$], and a contact ion pair (CIP) for [NBA–H⁺/$^1 3(O)^{-*}$].[25,29] The selectivity to form an SSIP or a CIP is determined by the basicity of BASE. Because the SSIP of $^1 3(O)^{-*}$ and
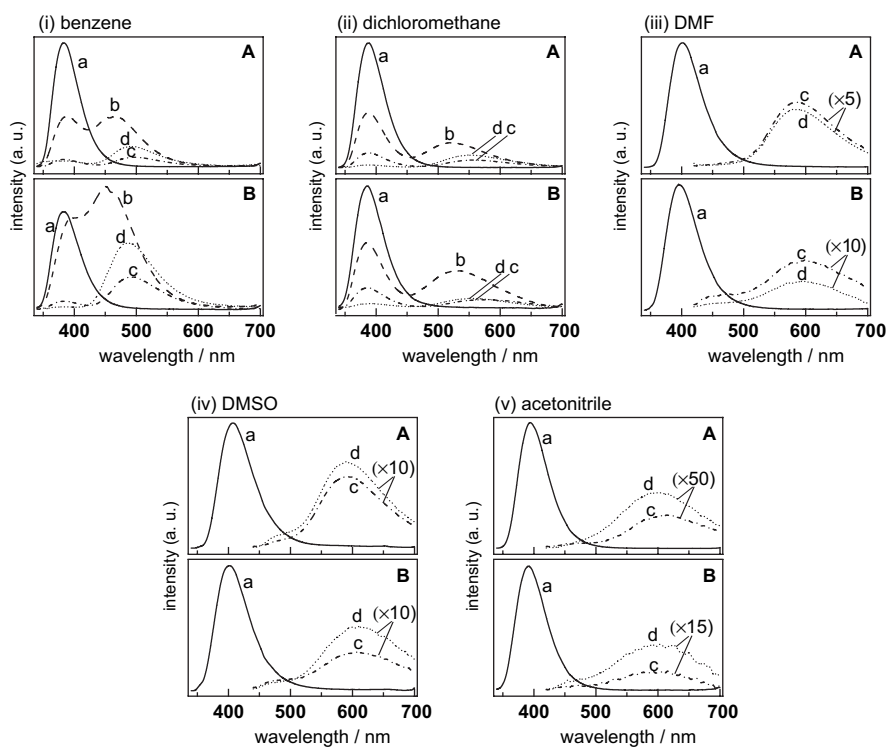

Figure 2. Fluorescence emission spectra of $3aH$ and [BASE–H⁺/$3a(O)^-$] (A) and $3bH$ and [BASE–H⁺/$3b(O)^-$] (B) in various solvents in the absence and presence of organic bases (1.0×10^{-2} mol L⁻¹) at 25 °C; organic base: none (a), NBA (b), TMG (c), and DBU (d). Selected solvents were benzene (i), dichloromethane (ii), DMF (iii), DMSO (iv), and acetonitrile (v). The initial concentrations of $3H$ were 1.5×10^{-6} mol L⁻¹, except for those (1.5×10^{-5} mol L⁻¹) in DMF, DMSO, and acetonitrile containing TMG and DBU. Excitation wavelengths (λ_{ex}) were 320 nm in benzene and dichloromethane. The λ_{ex} in DMF, DMSO, and acetonitrile were also 320 nm in the absence of the organic bases. The λ_{ex} in DMF and acetonitrile containing bases and in DMSO containing bases were 400 and 425 nm, respectively.
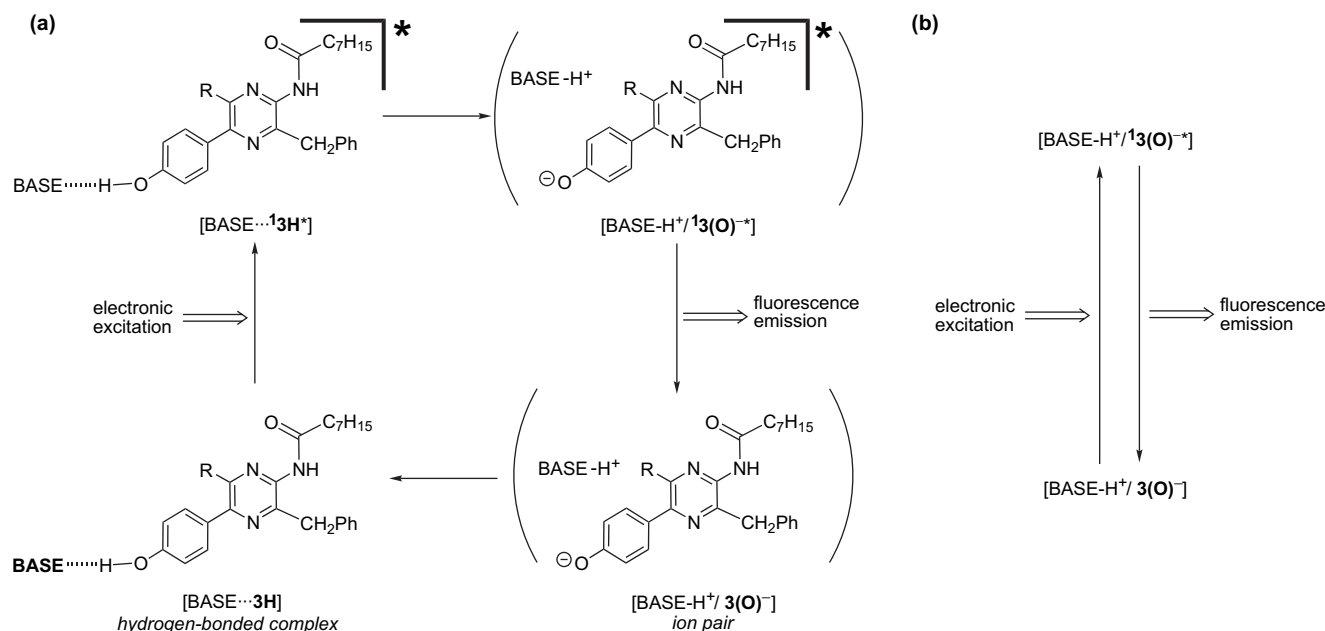
Scheme 6.

TMG–H^{+} or DBU–H^{+} is a loose ion pair separated by solvent molecules, the Coulomb force between $^1\mathbf{3(O)}^{-*}$ and TMG–H^{+} or DBU–H^{+} is weak and the fluorescence of $\mathbf{3(O)}^-$ is not much affected by the choice of BASE–H^{+}. On the other hand, the CIP of $^1\mathbf{3(O)}^{-*}$ and NBA–H^{+} holds together by an effective Coulomb force, and the degree of binding between $^1\mathbf{3(O)}^{-*}$ and NBA–H^{+} varies with the solvent polarity. Therefore, the molecular stability of $[\text{NBA–H}^+/^1\mathbf{3(O)}^{-*}]$ is sensitive to the solvent polarity, resulting in steep slopes of the E_{FL}–$E_{\text{T}}(30)$ correlations for $[\text{NBA–H}^+/\mathbf{3(O)}^-]$. Among a variety of combinations of $\mathbf{3(O)}^-$ and BASE–H^{+}, $[\text{NBA–H}^+/\mathbf{3(O)}^-]$ showed the highest Φ_f values (>0.1) in the solvent, with $E_{\text{T}}(30) < 38$ kcal mol^{-1}. This indicates that

$[\text{NBA–H}^+/^1\mathbf{3(O)}^{-*}]$ in a less polar solvent is favorable for increasing the Φ_f of $\mathbf{3(O)}^-$.

The slopes of the E_{FL}–$E_{\text{T}}(30)$ correlations for $[\text{BASE–H}^+/\mathbf{3b(O)}^-]$ are larger than the corresponding correlations for $[\text{BASE–H}^+/\mathbf{3a(O)}^-]$. This indicates that the degree of ICT in methyl derivative $^1\mathbf{3b(O)}^{-*}$ is enhanced by the twisted structure between 4-oxidophenyl and amidopyrazine moieties, as shown in Scheme 7. The stability of the twisted $^1\mathbf{3b(O)}^{-*}$ is more sensitive to the solvent polarity than is that of $^1\mathbf{3a(O)}^{-*}$, giving a steeper slope for the E_{FL}–$E_{\text{T}}(30)$ correlation for $[\text{BASE–H}^+/\mathbf{3b(O)}^-]$ than for $[\text{BASE–H}^+/\mathbf{3a(O)}^-]$. On the other hand, the Φ_f values of $\mathbf{3a(O)}^-$ and

Table 3. Fluorescence of **3aH** and its phenolate anion $\mathbf{3a(O)}^-$ in ion pairs with NBA–H^{+}, TMG–H^{+}, and DBU–H^{+} in various solvents at 25 °C

Solvent	$E_{\text{T}}(30)$/kcal mol^{-1}	λ_{FL}[a]/nm (Φ_f[b])			
		3aH[c]	**3aH**[c]+NBA[d] [NBA–H^{+}/**3a(O)**$^-$]	**3aH**[c]+TMG[d] [TMG–H^{+}/**3a(O)**$^-$]	**3aH**[c]+DBU[d] [DBU–H^{+}/**3a(O)**$^-$]
p-Xylene	33.1	383 (0.14)	452 (0.24)	490 (0.04)	486 (0.06)
Toluene	33.9	383 (0.17)	466 (0.23)	495 (0.03)	491 (0.06)
Benzene	34.3	383[e] (0.19)[e]	469[e] (0.27)[e]	498 (0.03)	490 (0.06)
Benzene/chloroform (20:1)	36.4	384 (0.19)	473 (0.23)	504 (0.03)	503 (0.05)
Chlorobenzene	36.8	385 (0.15)	501 (0.35)	542 (0.09)	531 (0.15)
Chloropropane	37.4	385 (0.17)	498 (0.19)	526 (0.10)	521 (0.12)
Benzene/chloroform (2:1)	38.0	387 (0.19)	499 (0.20)	527 (0.03)	522 (0.03)
1,2-Dichlorobenzene	38.0	385 (0.16)	505 (0.34)	537 (0.14)	530 (0.17)
Chloroform	39.1	389 (0.23)	500 (0.16)	542 (0.03)	542 (0.02)
Dichloromethane	40.7	388 (0.18)	518 (0.15)	557 (0.03)	553 (0.04)
1,2-Dichloroethane	41.3	388 (0.18)	520 (0.17)	554 (0.05)	544 (0.05)
Benzonitrile	41.5	394 (0.23)	546 (0.03)	562 (0.04)	554 (0.03)
DMAc	42.9	401 (0.22)	—[f]	575 (0.07)	575 (0.06)
DMF	43.2	402 (0.24)	—[f]	584[e] (0.04)[e]	583 (0.04)
Propionitrile	43.6	392 (0.20)	554 (0.02)	582 (0.02)	582 (0.01)
DMSO	45.1	408 (0.22)	—[f]	591[e] (0.02)[e]	590 (0.03)
Acetonitrile	45.6	394 (0.20)	—[f]	615[e] (0.01)[e]	598 (0.01)

[a] Fluorescence emission maxima. In the presence of the organic bases, only the λ_{FL} of the generated anion species are shown.
[b] Fluorescence quantum yields.
[c] The initial concentration of **3aH** was 1.5×10^{-6} mol L^{-1}.
[d] The initial concentration of the organic base was 1.0×10^{-2} mol L^{-1}.
[e] The value revised from the previous report (Ref. 28).
[f] No new emission band was observed in the presence of NBA.

Table 4. Fluorescence of **3bH** and its phenolate anion **3b(O)**⁻ in ion pairs with NBA–H⁺, TMG–H⁺, and DBU–H⁺ in various solvents at 25 °C

Solvent	$E_T(30)$/kcal mol⁻¹	λ_{FL}[a]/nm (Φ_f[b])			
		3bH[c]	**3bH**[c]+NBA[d] [NBA–H⁺/**3b(O)**⁻]	**3bH**[c]+TMG[d] [TMG–H⁺/**3b(O)**⁻]	**3bH**[c]+DBU[d] [DBU–H⁺/**3b(O)**⁻]
p-Xylene	33.1	383 (0.027)	444 (0.24)	480 (0.02)	479 (0.04)
Toluene	33.9	383 (0.031)	451 (0.30)	489 (0.02)	481 (0.04)
Benzene	34.3	384 (0.030)	451 (0.32)	494 (0.02)	488 (0.04)
Benzene/chloroform (20:1)	36.4	384 (0.029)	472 (0.16)	504 (0.02)	500 (0.03)
Chlorobenzene	36.8	384 (0.046)	480 (0.23)	522 (0.08)	515 (0.11)
1-Chloropropane	37.4	383 (0.026)	487 (0.09)	529 (0.04)	521 (0.05)
Benzene/chloroform (2:1)	38.0	385 (0.032)	504 (0.10)	540 (0.01)	534 (0.02)
1,2-Dichlorobenzene	38.0	385 (0.039)	501 (0.19)	542 (0.11)	531 (0.10)
Chloroform	39.1	385 (0.032)	514 (0.07)	560 (0.01)	556 (0.01)
Dichloromethane	40.7	386 (0.025)	530 (0.04)	578 (<0.005)	552 (<0.005)
1,2-Dichloroethane	41.3	384 (0.031)	527 (0.07)	562 (0.01)	552 (0.02)
Benzonitrile	41.5	394 (0.080)	557 (0.02)	570 (0.01)	557 (0.02)
DMAc	42.9	395 (0.052)	—[e]	572 (0.01)	582 (0.01)
DMF	43.2	396 (0.052)	—[e]	602 (0.01)	597 (0.01)
Propionitrile	43.6	391 (0.027)	566 (<0.005)	585 (0.01)	576 (0.01)
DMSO	45.1	402 (0.065)	—[e]	610 (0. 01)	607 (0.01)
Acetonitrile	45.6	391 (0.025)	—[e]	600 (<0.005)	595 (<0.005)

[a] Fluorescence emission maxima. In the presence of the organic bases, only the λ_{FL} of the generated anion species are shown.
[b] Fluorescence quantum yields.
[c] The initial concentration of **3bH** was 1.5×10^{-6} mol L⁻¹.
[d] The initial concentration of the organic base was 1.0×10^{-2} mol L⁻¹.
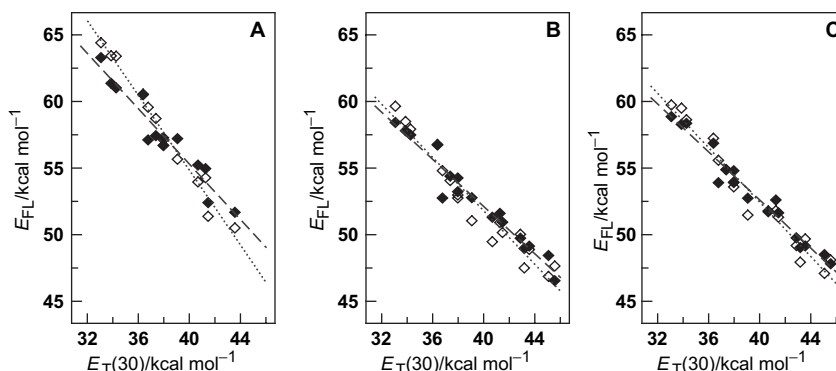[e] No new emission band was observed in the presence of NBA.

Figure 3. Plots of E_{FL} (in kcal mol⁻¹) for **3a(O)**⁻ (◆) and **3b(O)**⁻ (◇) in ion pairs with NBA–H⁺ (A), TMG–H⁺ (B), and DBU–H⁺ (C) against $E_T(30)$ (in kcal mol⁻¹).

3b(O)⁻ were similar to each other, while **3aH** and **3bH** had different Φ_f values. This result indicates that the methyl group at C6 in **3b(O)**⁻ does not enhance a non-radiative process from the twisted ¹**3b(O)**⁻*, which competes with the fluorescence emission process. Excited neutral molecules ¹**3H***, however, are affected by the methyl substitution, whose steric effect causes a decrease of Φ_f.

¹**3a(O)**⁻*: R = H
¹**3b(O)**⁻*: R = CH₃
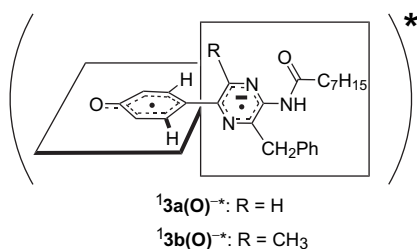
Scheme 7.

Because the E_{FL}–$E_T(30)$ correlations for **3a(O)**⁻ in the ion pairs were revised from the previous one,[27] we recompared the E_{FL}–$E_T(30)$ correlations for [BASE–H⁺/**3a(O)**⁻] with that for a dimethylamino analogue **6**, $E_{FL}=-0.64E_T(30)+85$ ($r=-0.98$).[16] The slopes of the E_{FL}–$E_T(30)$ correlations for [BASE–H⁺/**3a(O)**⁻] are all steeper than those for **6**, while the intercepts of the E_{FL}–$E_T(30)$ correlations for [TMG–H⁺/**3a(O)**⁻] or [DBU–H⁺/**3a(O)**⁻] and **6** are similar to each other. The different slopes for [BASE–H⁺/**3a(O)**⁻] and **6** are related to the electron-donating abilities of the oxido and dimethylamino groups, respectively. The modified Hammett constant σ_p^+ for the oxido group (−2.30) is smaller than that of the dimethylamino group (−1.70).[30,31] Therefore, the oxido group plays an important role as an electron donor for stabilizing the ICT state of ¹**3a(O)**⁻* (Scheme 7).

6
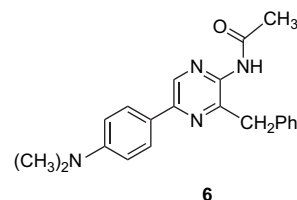
2.3. Luminescent properties of amide anion 5(N)⁻: chemiluminescence of coelenterazine analogue 4 in various solvents

To consider the difference in the fluorescent properties between $2(O)^-$ and $2(N)^-$, we investigated the fluorescence of amide anion $5(N)^-$ generated from **5H** with a strong base, such as NaOH, in a polar solvent with strong ionizing power, such as DMSO.[32] Unfortunately, reproducible fluorescence data were not obtained for $5(N)^-$ in a solvent with a low ionizing power such as benzene, because of interferences from side reactions. The difficulty in observing $5(N)^-$ is caused by the low acidity of the amide moiety in **5H**.[19–21]

To evaluate the fluorescent properties of $5(N)^-$ in an ion pair in various solvents, we investigated the chemiluminescence of **4**, which showed the fluorescence emission from [BASE–H^+/$^1 5(N)^{-*}$] (Scheme 8). Chemiluminescence of **4** was easily observed in aerated DMSO and DMF (Fig. 4), and the fluorescence emission maxima (λ_{FL}) of [DMSO–H^+/$5(N)^-$] and [DMF–H^+/$5(N)^-$] almost reproduced the reported data.[12,32–34] On the other hand, **4** did not react in aerated benzene, dichloromethane, or acetonitrile in the absence of a base. TMG was used as an organic base in these solvents to initiate a chemiluminescence reaction of **4**[35] and the fluorescence emission from [TMG–H^+/$^1 5(N)^{-*}$]
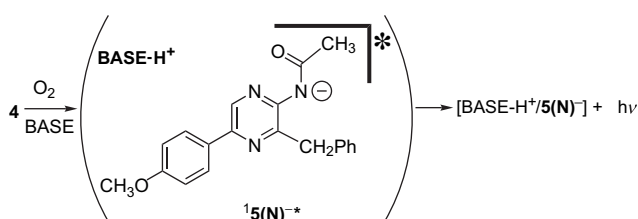
was observed, as shown in Figure 4. In benzene, an emission from excited neutral molecule $^1 5H^*$ also appeared around 400 nm. The λ_{FL} values and chemiluminescence quantum yields (Φ_{cl}) are summarized in Table 5. The Φ_{cl} values in benzene, dichloromethane, and acetonitrile were smaller than those in DMSO and DMF. The λ_{FL} values of [BASE–H^+/$5(N)^-$] were in the range of 464–476 nm, which is less than that of [BASE–H^+/$3a(O)^-$]. The λ_{FL} values of [BASE–H^+/$5(N)^-$] did not depend on the BASE–H^+, which were DMSO–H^+, DMF–H^+, and TMG–H^+. Therefore, the fluorescence of $5(N)^-$ was not significantly affected by the interaction with BASE–H^+ in the ion pair or the solvent polarity.

Table 5. Emission maxima (λ_{FL}) and quantum yields (Φ_{cl}) for the chemiluminescence of **4** in various solvents under air

Solvent	Additive	λ_{FL}/nm	$\Phi_{cl}/10^{-3}$
Benzene	TMG[a]	464	0.005
Dichloromethane	TMG[a]	470	0.02
DMF	None	471	1.5
DMSO	None	476	1.1
Acetonitrile	TMG[a]	473	0.06

[a] The concentration of TMG was 1.0×10^{-2} mol L⁻¹.

2.4. Molecular orbital calculations for the ground and the singlet-excited states of anion species of a coelenteramide analogue

To gain insight into the structural characteristics of $2(O)^-$ and $2(N)^-$, we carried out PM5 semi-empirical molecular orbital (MO) calculations for the ground and the singlet-excited states of $7(O)^-$ and $7(N)^-$, which are the anion species of an acetamide analogue (Tables 6 and 7). Because the stabilities of ionic molecules are affected by dielectric molecular environments, we performed the calculations with the COSMO method[36] using several dielectric constants (ε).[25]

Scheme 8.

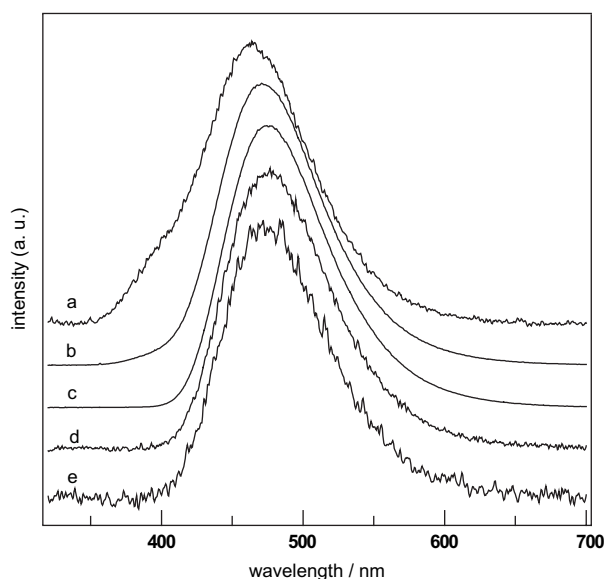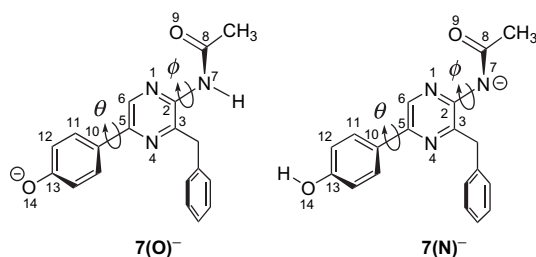**Figure 4**. Chemiluminescence spectra of **4** (1.5×10^{-5} mol L⁻¹) in various solvents under air. Solvents were benzene containing TMG (a), dichloromethane containing TMG (b), DMF (c), DMSO (d), and acetonitrile containing TMG (e). Concentrations of TMG were 1.0×10^{-2} mol L⁻¹.

In the ground state, it is reasonable that the heats of formation (ΔH_f) of $7(O)^-$ are smaller than those of $7(N)^-$ under various dielectric conditions, because the acidity of a phenolic hydroxy group is higher than that of an amide moiety in general.[18,19] The HOMO–LUMO energy gaps of $7(O)^-$ were predicted to be smaller than those of $7(N)^-$. The torsion angles C6–C5–C10–C11 (θ) and N1–C2–N7–C8 (ϕ) of $7(O)^-$ and $7(N)^-$ indicate that the conformations of the pyrazine rings with the 4-oxido- or 4-hydroxyphenyl group and with the amide moiety are twisted, but neither perpendicular nor coplanar. As the characteristic bond lengths in $7(O)^-$ and $7(N)^-$, the C13–O14 of $7(O)^-$ is shortened by the conjugation of the oxido group to the phenyl group, while the C8=O9 of $7(N)^-$ is elongated by the conjugation

Table 6. Calculated properties of $\mathbf{7(O)}^-$ and $\mathbf{7(N)}^-$ in the ground state with the PM5-COSMO method

Compounds	ε^a	$\Delta H_f{}^b$/kJ mol^{-1}	HOMO/eV	LUMO/eV	$\Delta E_{\text{HOMO–LUMO}}{}^c$/eV	θ^d/°	ϕ^d/°	r(C=O)^e/Å	r(C–O)^e/Å	r(C–C)^e/Å
$\mathbf{7(O)}^-$	2.27	−405	−6.06	0.61	6.67	155.5	113.1	1.235	1.271	1.444
	8.93	−593	−8.09	−0.73	7.26	142.7	42.4	1.247	1.298	1.461
	35.94	−664	−8.76	−1.14	7.62	140.5	37.8	1.253	1.309	1.464
	46.45	−669	−8.81	−1.17	7.64	141.0	39.7	1.254	1.309	1.465
$\mathbf{7(N)}^-$	2.27	−396	−6.92	1.07	7.99	43.6	114.0	1.262	1.358	1.468
	8.93	−567	−8.53	−0.33	8.20	47.6	73.0	1.278	1.354	1.469
	35.94	−627	−8.95	−0.85	8.10	46.3	68.4	1.284	1.353	1.468
	46.45	−632	−9.01	−0.90	8.11	45.5	75.1	1.285	1.352	1.468

[a] Dielectric constants at 25 °C of benzene (2.27), dichloromethane (8.93), acetonitrile (35.94), and DMSO (46.45) from Ref. 25.
[b] Heat of formation.
[c] HOMO–LUMO energy gap.
[d] The angles θ and ϕ are torsion angles C6–C5–C10–C11 and N1–C2–N7–C8, respectively.
[e] The r(C=O), r(C–O), and r(C–C) are the bond lengths of C8–C9, C13–O14, and C5–C10, respectively.

of the amide anion. The C5–C10 of $\mathbf{7(O)}^-$ and $\mathbf{7(N)}^-$ are the lengths of typical single bonds. The calculated structures of $\mathbf{7(O)}^-$ with a twisted conformation between the 4-oxidophenyl and the pyrazine moieties and the C5–C10 single bond predict that $\mathbf{2(O)}^-$ has little proportion of a quinoid form (Scheme 3c) in the resonance structures.

The data of $^1\mathbf{7(O)}^{-*}$ and $^1\mathbf{7(N)}^{-*}$ calculated with the PM5-CI-COSMO method (Table 7) indicate that the ΔH_f values of $^1\mathbf{7(O)}^{-*}$ are much smaller than those of $^1\mathbf{7(N)}^{-*}$ under various dielectric conditions. The difference in ΔH_f between $^1\mathbf{7(O)}^{-*}$ and $^1\mathbf{7(N)}^{-*}$, 105–159 kJ mol^{-1}, is much larger than that between $\mathbf{7(O)}^-$ and $\mathbf{7(N)}^-$, 9–37 kJ mol^{-1}, suggesting that the difference in the acidities between the phenolic hydroxy group and the amide moiety in the singlet-excited state is much larger than that in the ground state. Thus, the phenolic hydroxy group is the most acidic moiety in $^1\mathbf{2H}^{*}$.[18] As structural characteristics, the θ values of $^1\mathbf{7(O)}^{-*}$ and $^1\mathbf{7(N)}^{-*}$ are close to 90°, except the θ value of $^1\mathbf{7(N)}^{-*}$ with $\varepsilon=2.27$ (benzene). The C8=O9 and C5–C10 of $^1\mathbf{7(O)}^{-*}$ and $^1\mathbf{7(N)}^{-*}$ show a small difference from those of the corresponding ground states, while their C13–O14 becomes slightly short. The calculated structure of $^1\mathbf{7(O)}^{-*}$ with the perpendicular conformation between the 4-oxidophenyl and the pyrazine moieties is consistent with the twisted structure of $^1\mathbf{3(O)}^{-*}$ (Scheme 7) concluded from the fluorescence observations. This result also indicates that $^1\mathbf{2(O)}^{-*}$ does not have the property of a quinoid form (Scheme 3c).

Table 8 shows the summations of the net atomic charge ($\sum q$) at the four parts of $\mathbf{7(O)}^-$ and $^1\mathbf{7(O)}^{-*}$: the

4-oxidophenyl (**A**), pyrazine (**B**), acetamide (**C**), and benzyl (**D**). The negative charge in $\mathbf{7(O)}^-$ is mainly localized at the 4-oxidophenyl group. On the other hand, the $\sum q$ values at the pyrazine and the acetamido parts of $^1\mathbf{7(O)}^{-*}$ were below −0.86 and −0.13, respectively, indicating that the negative

Table 8. Summations of the net atomic charges ($\sum q$) at the 4-oxidophenyl (A), pyrazine (B), acetamide (C), and benzyl (D) parts of $\mathbf{7(O)}^-$ and $^1\mathbf{7(O)}^{-*}$, calculated with the PM5-COSMO and the PM5-CI-COSMO methods, respectively
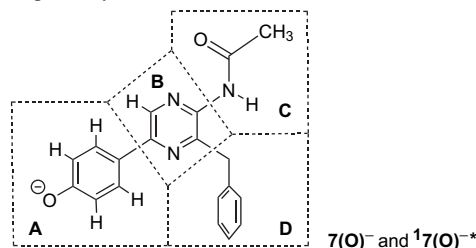
Compounds	ε^a	Summations of the net atomic charges ($\sum q$)			
		A	B	C	D
$\mathbf{7(O)}^-$	2.27	−0.814	−0.228	−0.082	+0.124
	8.93	−0.898	−0.199	−0.051	+0.148
	35.94	−0.917	−0.203	−0.039	+0.158
	46.45	−0.918	−0.204	−0.037	+0.159
$^1\mathbf{7(O)}^{-*}$	2.27	−0.056	−0.863	−0.157	+0.076
	8.93	−0.045	−0.920	−0.137	+0.102
	35.94	−0.034	−0.949	−0.134	+0.117
	46.45	−0.028	−0.957	−0.133	+0.118

[a] Dielectric constants at 25 °C of benzene (2.27), dichloromethane (8.93), acetonitrile (35.94), and DMSO (46.45) from Ref. 25.

Table 7. Calculated properties of $\mathbf{7(O)}^-$ and $\mathbf{7(N)}^-$ in the singlet-excited states ($^1\mathbf{7(O)}^{-*}$ and $^1\mathbf{7(N)}^{-*}$) with the PM5-CI-COSMO method

Compounds	ε^a	$\Delta H_f{}^b$/kJ mol^{-1}	θ^c/°	ϕ^c/°	r(C=O)^d/Å	r(C–O)^d/Å	r(C–C)^d/Å
$^1\mathbf{7(O)}^{-*}$	2.27	−243	90.2	93.8	1.238	1.243	1.461
	8.93	−413	92.3	64.5	1.252	1.259	1.455
	35.94	−470	91.8	49.9	1.254	1.267	1.453
	46.45	−476	91.7	51.0	1.255	1.268	1.452
$^1\mathbf{7(N)}^{-*}$	2.27	−84	26.5	44.9	1.250	1.357	1.437
	8.93	−261	92.8	114.6	1.283	1.295	1.453
	35.94	−363	94.1	114.9	1.287	1.291	1.457
	46.45	−371	94.0	115.4	1.287	1.290	1.457

[a] Dielectric constants at 25 °C of benzene (2.27), dichloromethane (8.93), acetonitrile (35.94), and DMSO (46.45) from Ref. 25.
[b] Heat of formation.
[c] The angles θ and ϕ are torsion angles C6–C5–C10–C11 and N1–C2–N7–C8, respectively.
[d] The r(C=O), r(C–O), and r(C–C) are the bond lengths of C8–C9, C13–O14, and C5–C10, respectively.

charge localized at the amidopyrazine moiety in the singlet-excited state. These results predict that the negative charge of $7(O)^-$ is transferred from the 4-oxidophenyl group to the amidopyrazine moiety upon electronic excitation, and strongly support that $^1 2(O)^{-*}$ is the twisted ICT state (Scheme 7). The amidopyrazine moiety of $2(O)^-$ is the center of the fluorescent chromophore and has a localized negative charge in the singlet-excited state. Therefore, a solvation of the amidopyrazine moiety of $^1 2(O)^{-*}$ by polar solvent molecules will effectively increase its molecular stability, resulting in a decreased transition energy from $^1 2(O)^{-*}$ to $2(O)^-$. This causes the solvent-dependent spectral shift of the fluorescence of $2(O)^-$, which is observed as the steep slopes of the E_{FL}–$E_T(30)$ correlations for $[BASE–H^+/3(O)^-]$.

2.5. Bioluminescence light emitter and the reaction mechanism of the calcium-activated photoproteins
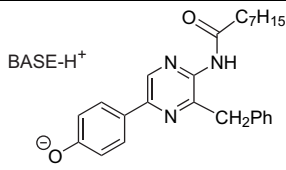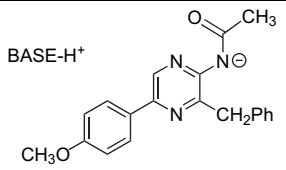
The fluorescent properties of $[BASE–H^+/3a(O)^-]$ and $[BASE–H^+/5(N)^-]$ are summarized in Table 9. The reported emission maxima (λ_{BL}) of the bioluminescence of aequorin and obelin are in the ranges of 465–470 nm[11a,37] and 485–495 nm[38], respectively. Both ranges are covered by the λ_{FL} range of $[BASE–H^+/3a(O)^-]$, 452–615 nm, but not by that of $[BASE–H^+/5(N)^-]$, 464–476 nm. The λ_{FL} range of $[NBA–H^+/3a(O)^-]$, 452–554 nm, especially covers these λ_{BL} ranges, while that of $[TMG–H^+/3a(O)^-]$ and $[DBU–H^+/3a(O)^-]$, 486–615 nm, is red shifted compared with the λ_{BL} range of aequorin. These results support the fact that the real ionic structure of the excited coelenteramide in the bioluminescence of aequorin and obelin is $^1 2(O)^{-*}$ in a CIP, with a counter cation composed of a side chain of an amino acid. The large spectral variation in the fluorescence of $3a(O)^-$ is caused by the molecular stability change of $^1 3a(O)^{-*}$ at the twisted ICT state, depending on the ion pair structure and the solvent polarity.

The X-ray crystal structures of aequorin[6,39] and obelin[7] indicate that their active sites are composed of hydrophobic α-helices and the substrates are surrounded by tryptophans, tyrosines, histidines, and phenylalanines. Furthermore, the imidazolium side chains of His 16 in aequorin and His 22 in obelin are able to be counter cations for the 4-oxidophenyl group of $^1 2(O)^{-*}$. Because the imidazole part of the histidine side chain is a weak organic base (pK_a of the conjugated acid

of imidazole: 14.2 in acetonitrile[40]), $^1 2(O)^{-*}$ and the imidazolium cation will make a CIP such as $[NBA–H^+/^1 3(O)^{-*}]$ at the active sites in aequorin and obelin. By applying the E_{FL}–$E_T(30)$ correlation for $[NBA–H^+/3a(O)^-]$ to evaluate the λ_{BL} of aequorin bioluminescence (465–470 nm), we can predict that the active site in aequorin has a polarity similar to benzene ($E_T(30)=34.3$), as predicted in previous reports.[17] The E_{FL}–$E_T(30)$ correlation for $[NBA–H^+/3b(O)^-]$ is also useful for evaluating the reported λ_{BL} of a semi-synthetic aequorin, $m(5)$-aequorin, prepared using 5-methylcoelenterazine analogue. The λ_{BL} of $m(5)$-aequorin (438–440 nm)[24] is similar to the λ_{FL} (444 nm) of $[NBA–H^+/3b(O)^-]$ in p-xylene ($E_T(30)=33.1$), also supporting the less polar character of the active site in aequorin. The λ_{BL} of obelin bioluminescence (485–495 nm) predicts that the active site has a polarity intermediate between a mixed solvent of benzene/chloroform (20:1) ($E_T(30)=36.4$) and 1-chloropropane ($E_T(30)=37.4$). Thus, aequorin and obelin have less polar active sites, where the CIP of $^1 2(O)^{-*}$ and the imidazolium side chain show a high Φ_f. Based on these evaluations and the X-ray crystal structures of aequorin[6,39] and obelin,[7] we can draw a schematic representation of the important interactions of $^1 2(O)^{-*}$ with the active site in aequorin or obelin, shown in Scheme 9.

The conclusion that $^1 2(O)^{-*}$ in the CIP is the light emitter in aequorin and obelin bioluminescence leads us to propose a bioluminescence reaction mechanism (Scheme 10) including the active site structures of aequorin[6,39] and obelin.[7] Because $^1 2(O)^{-*}$ in the CIP is the primary excited product, we can propose that the chemiexcitation process is a thermal decomposition of the NH-form of dioxetanone intermediate 11^- possessing a 4-oxidophenyl group.[41] The chemiexcitation from 11^- to $^1 2(O)^{-*}$ in the CIP would be an important process to achieve the high quantum yield in the bioluminescence reaction. On the whole, a structural change of the active site due to chelation of Ca^{2+} ions with the EF-hands induces the conversion of coelenterazine 2-hydroperoxide 8 to a reactive peroxide anion (9^{2-}), followed by a cyclization to an unstable amine anion form of dioxetanone intermediate 10^{2-}. Dioxetanone dianion 10^{2-} receives a proton from a neighboring 4-hydroxyphenyl group of a tyrosine residue (Y132 and Y138 for aequorin and obelin, respectively) in the active site to give 11^-. Then, the chemiexciation from 11^- to $^1 2(O)^{-*}$ and the light emission from $^1 2(O)^{-*}$ lead to FLP, which contains the hydrogen-bonded complex

Table 9. Comparison of the fluorescent properties of $[BASE–H^+/3a(O)^-]$ and $[BASE–H^+/5(N)^-]$

$[BASE–H^+/3a(O)^-]$ $[BASE–H^+/5(N)^-]$

	$[BASE–H^+/3a(O)^-]$	$[BASE–H^+/5(N)^-]$
Character of the singlet-excited state of the anion	Twisted ICT state	Normal π–π^* state
Variation of λ_{FL} depending on the solvent polarity (observed λ_{FL} range)	Large (452–615 nm)	Small (464–476 nm)
Variation of λ_{FL} depending on the ion pair structure	Large (SSIP vs CIP)	Small
High Φ_f condition	In a CIP with a conjugate acid of a weak base such as n-butylamine in a less polar solvent	0.2 in DMSO
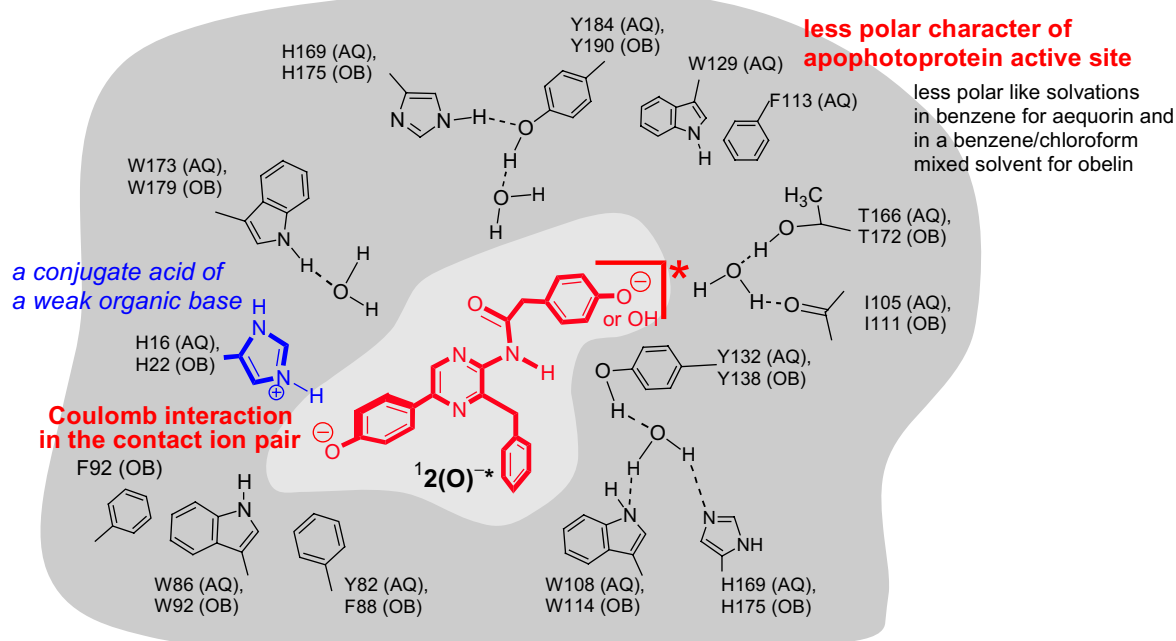
Scheme 9. (AQ=aequorin, OB=obelin).
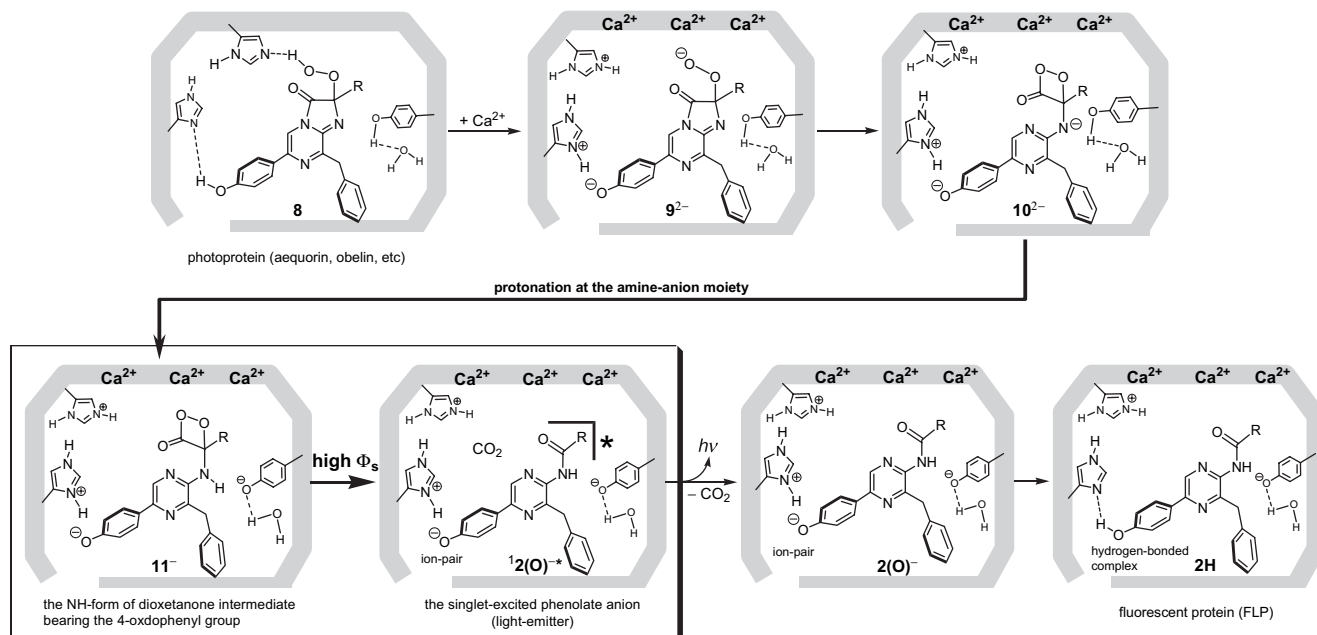
Scheme 10. R=(4-hydroxyphenyl)methyl or (4-oxidophenyl)methyl.

of **2H** with an imidazole side chain of a histidine residue (H16 and H22 for aequorin and obelin, respectively). Electronic excitation of FLP gives $^1\mathbf{2(O)}^{-*}$ in the CIP with the imidazolium side chain by the process illustrated in Scheme 6a, and shows a fluorescence emission spectrum identical to the bioluminescence spectrum. The molecular mechanism shown in Scheme 10 is common in the bioluminescence system of calcium-activated photoproteins.[1,42]

3. Conclusion

The fluorescent properties of [BASE–H⁺/**3(O)**⁻] and [BASE–H⁺/**5(N)**⁻] were systematically investigated to

elucidate the ionic structure of the light emitter in aequorin and obelin bioluminescences. The fluorescence of [BASE–H⁺/**3(O)**⁻] was observed by an electronic excitation of [BASE–H⁺/**3(O)**⁻] or [BASE···**3H**] in a polar or a less polar solvent (Scheme 6). Because the fluorescence emission from $^1\mathbf{3(O)}^{-*}$ in an ion pair has an ICT nature, the λ_{FL} of [BASE–H⁺/**3(O)**⁻] was evaluated with linear E_{FL}–$E_T(30)$ correlations. A comparison of the E_{FL}–$E_T(30)$ correlations and the Φ_f values among the ion pairs of **3(O)**⁻ with NBA–H⁺, TMG–H⁺, and DBU–H⁺ clarified that the fluorescence of **3(O)**⁻ was affected by a structural variation of an ion pair: an SSIP for [TMG–H⁺/$^1\mathbf{3(O)}^{-*}$] or [DBU–H⁺/$^1\mathbf{3(O)}^{-*}$], and a CIP for [NBA–H⁺/$^1\mathbf{3(O)}^{-*}$]. [NBA–H⁺/$^1\mathbf{3(O)}^{-*}$]

showed especially steep E_{FL}–E_T(30) correlations and high Φ_f compared with those of [TMG–H$^+$/^{1}3(O)$^{-*}$] and [DBU–H$^+$/^{1}3(O)$^{-*}$]. Comparison of the fluorescent properties of 3a(O)$^-$ and 3b(O)$^-$ in ion pairs clarified that ^{1}3(O)$^{-*}$ is the twisted ICT state with a localized negative charge at the amidopyrazine moiety (Scheme 7). This was supported by PM5-CI-COSMO calculations for ^{1}7(O)$^{-*}$. The fluorescence emission from [BASE–H$^+$/^{1}5(N)$^{-*}$] generated by the chemiluminescence reactions of 4 indicates that the fluorescence of [BASE–H$^+$/5(N)$^-$] is not significantly affected by interaction with BASE–H$^+$ in the ion pair or the solvent polarity. These results confirm that ^{1}2(O)$^{-*}$ in a CIP is the light emitter in the bioluminescence of the representative calcium-activated photoproteins, aequorin and obelin. The E_{FL}–E_T(30) correlations for [NBA–H$^+$/3(O)$^-$] were applied to evaluate the λ_{BL} values of aequorin and obelin bioluminescences, suggesting that the active sites of these photoproteins have a polarity similar to a less polar solvent such as benzene. The CIP of ^{1}2(O)$^{-*}$ with an imidazolium side chain of a histidine residue in the less polar active site is a good state for a high Φ_f of 2(O)$^-$ in apoprotein. The predicted character of the active sites of aequorin and obelin is consistent with their structural characteristics established by X-ray crystallographic analyses of aequorin[6,39] and obelin[7] (Scheme 9). The conclusion that ^{1}2(O)$^{-*}$ in the CIP is the light emitter indicates that ^{1}2(O)$^{-*}$ is the primary product of the bioluminescence reaction. Therefore, we propose a bioluminescence reaction mechanism including the chemiexcitation from dioxetanone intermediate 11$^-$ to ^{1}2(O)$^{-*}$ (Scheme 10). Further study to establish the reaction mechanism is now in progress in our lab.

4. Experimental

4.1. General

Melting points were obtained with a Yamato MP-21 apparatus and were uncorrected. IR spectra were measured with a Horiba FT-720 spectrometer. Electron ionization (EI) mass spectra were recorded with a JEOL JMS-600 mass spectrometer. High-resolution EI and electro-spray ionization (ESI) mass spectra were recorded with a JEOL HX-110 and a Bruker-Daltonics APEX III mass spectrometer, respectively, at the Research Centre for Giant Molecules, Graduate School of Science, Tohoku University. ^{1}H and ^{13}C NMR spectra were recorded on a JEOL GX-270 instrument (270 and 67.8 MHz, respectively). UV–vis absorption spectra were measured with a Varian Cary 50 spectrophotometer (scan speed, 200 nm min^{-1}; data interval, 0.33 nm). Fluorescence spectra were measured with a JASCO FP-6500 fluorescence spectrophotometer (excitation and emission bandpasses, 3 nm; scan speed, 200 nm min^{-1}) and were corrected according to manufacturer's instructions. Fluorescence quantum yields were determined relative to quinine sulfate in 0.10 mol L^{-1} H$_2$SO$_4$ (Φ_F=0.55, λ_{ex} 366 nm) as the standard. Chemiluminescence spectra were measured with an ATTO AB-1850 spectrophotometer. Spectroscopic measurements were made in a quartz cuvette (1 cm path length) at 25±1 °C. Spectral-grade solvents were used for measurements of UV–vis absorption, fluorescence, and chemiluminescence emission spectra. The intensity of the total light (400–700 nm) emitted from a chemilumi-

nescence reaction was monitored using a Hamamatsu R5929 photomultiplier tube powered by a Hamamatsu C4900 power supply. The signal from the photomultiplier was collected on a PC computer and the data were analyzed with the graphic program Igor Pro, Version 4.0.8.0 (Wave Metrics, Inc.). Semi-empirical MO calculations for ground and singlet-excited states were carried out with the PM5 and PM5-CI methods[43] and the COSMO model[36] of CAChe Ver. 5.04 for Windows (Fujitsu Ltd, Tokyo, Japan, 2002). The geometries of ground state molecules were fully optimized by the MM2 calculations before PM5 calculations. Geometries of singlet-excited molecules were optimized using the keywords excited singlet cisd c.i.=4 root=2.

4.2. Preparation of coelenteramide and coelenterazine derivatives

Coelenteramide analogue 3aH [3-benzyl-5-(4-hydroxyphenyl)-2-octanamidopyrazine] and coelenterazine analogue 4 [8-benzyl-6-(4-hydroxyphenyl)-2-methylimidazo[1,2-a]-pyrazin-3(7H)-one] were prepared by reported procedures.[16,17b,44] Coelenteramide analogue 3bH [3-benzyl-5-(4-hydroxyphenyl)-6-methyl-2-octanamidopyrazine] was synthesized from 6-methylpyrazinamine as follows (Scheme 4).

4.2.1. 3,5-Dibromo-6-methylpyrazinamine.
To a solution of 6-methylpyrazinamine[45] (0.97 g, 8.8 mmol) in CHCl$_3$ (30 mL) and pyridine (3.5 mL) was added tetra-n-butyl-ammonium tribromide (10.5 g, 0.21 mol) under Ar. The reaction mixture was heated under reflux for 2 h. After cooling, the mixture was concentrated under reduced pressure. The residue was diluted with water (100 mL) and the product was extracted with ether (200 mL×4). The ether phase was washed with saturated brine, dried over anhydrous Na$_2$SO$_4$, and concentrated under reduced pressure. The residue was purified by silica gel column chromatography (CHCl$_3$), yielding 3,5-dibromo-6-methylpyrazinamine (1.10 g, 46%) as pale yellow cubes: mp 167–168 °C; ^{1}H NMR (CDCl$_3$) δ 4.93 (br s, 2H), 2.46 (s, 3H); IR (KBr) 3499, 3292, 3155, 1632, 1540, 1448 cm^{-1}; MS (EI, 70 eV) m/z (%) 269 (49), 267 (M$^+$, 100), 265 (51); HRMS (ESI) calcd for C$_5$H$_6$Br$_2$N$_3$ 265.8928; found 265.8923 (M+H$^+$).

4.2.2. 3-Benzyl-5-bromo-6-methylpyrazinamine.
A solution of 3,5-dibromo-6-methylpyrazinamine (114 mg, 0.43 mmol), benzyltri-n-butyltin (195 mg, 0.51 mmol) and PdCl$_2$(PPh$_3$)$_2$ (15 mg, 5 mol %) in DMF (1 mL) was heated at 130 °C for 2.5 h under Ar. After cooling, the solution was concentrated under reduced pressure. The residue was dissolved in a saturated KF solution in methanol (7 mL) and the mixture was stirred for 1 h at room temperature. The reaction mixture was directly adsorbed on silica gel (5 g) and purified by silica gel column chromatography (CHCl$_3$/ethyl acetate=20:1), yielding 3-benzyl-5-bromo-6-methylpyrazinamine (43 mg, 36%) as pale yellow cubes: mp 94.5–95.5 °C; ^{1}H NMR (CDCl$_3$) δ 7.20–7.36 (m, 5H), 4.28 (br s, 2H), 4.06 (s, 2H), 2.49 (s, 3H); IR (KBr) 3465, 3305, 3165, 1633, 1602, 1533, 1429 cm^{-1}; MS (EI, 70 eV) m/z (%) 279 (98), 277 (M$^+$, 100), 276 (41), 198 (25), 130 (26); HRMS (ESI) calcd for C$_{12}$H$_{13}$BrN$_3$ 278.0293; found 278.0287 (M+H$^+$).

4.2.3. 3-Benzyl-5-(4-benzyloxyphenyl)-6-methylpyrazin-amine. A solution of 3-benzyl-5-bromo-6-methylpyrazin-amine (64 mg, 0.23 mmol), 4-benzyloxyphenylboronic acid (78 mg, 0.34 mmol), and Pd(PPh$_3$)$_4$ (13 mg, 5 mol %) in 1,4-dioxane (1.2 mL) and 2 mol L^{-1} Na$_2$CO$_3$ aqueous solution (1.2 mL) was heated at 110 °C for 2 h under Ar. After cooling, the mixture was diluted with water and the product was extracted with ethyl acetate (20 mL×3). The organic phase was washed with saturated brine, dried over anhydrous Na$_2$SO$_4$, and concentrated under reduced pressure. The residue was purified by silica gel column chromatography (CHCl$_3$/ethyl acetate=5:1), yielding 3-benzyl-5-(4-benzyloxyphenyl)-6-methylpyrazinamine (58 mg, 94%) as pale yellow powder: mp 125.5–126.5 °C; ^{1}H NMR (CDCl$_3$) δ 7.50 (AA′BB′, 2H), 7.21–7.45 (m, 10H), 7.06 (AA′BB′, 2H), 5.13 (s, 2H), 4.29 (br s, 2H), 4.19 (s, 2H), 2.45 (s, 3H); IR (KBr) 3478, 3303, 3168, 1633, 1610, 1449, 1425 cm^{-1}; MS (EI, 70 eV) m/z (%) 382 (19), 381 (M$^+$, 65), 290 (100); HRMS (ESI) calcd for C$_{25}$H$_{24}$N$_3$O 382.1919; found 382.1914 (M+H$^+$).

4.2.4. 3-Benzyl-5-(4-benzyloxyphenyl)-6-methyl-2-octa-namidopyrazine. To a solution of 3-benzyl-5-(4-benzyl-oxyphenyl)-6-methylpyrazinamine (45 mg, 0.12 mmol) and pyridine (0.2 mL) in dichloromethane (2 mL) was added octanoyl chloride (70 μL, 0.42 mmol) at 0 °C under Ar, and allowed to warm up to ambient temperature for 90 min. The reaction was quenched by the addition of saturated NaHCO$_3$ aqueous solution and the product was extracted with CHCl$_3$. The organic layer was washed with brine, dried over Na$_2$SO$_4$, and concentrated in vacuo. The residue was purified by silica gel column chromatography (CHCl$_3$/ethyl acetate=10:1), yielding 3-benzyl-5-(4-benzyloxyphenyl)-6-methyl-2-octanamidopyrazine (31 mg, 52%) as colorless powder: mp 156–157 °C; ^{1}H NMR (270 MHz, CDCl$_3$) δ 7.54 (AA′BB′, 2H), 7.16–7.48 (m, 10H), 7.07 (AA′BB′, 2H), 5.14 (s, 2H), 4.23 (s, 2H), 2.55 (s, 3H), 2.36 (t, J=7.6 Hz, 2H), 1.30 (m, 10H), 0.89 (t, J=6.9 Hz, 3H); IR (KBr) 3274, 2926, 2854, 1668, 1608, 1567, 1496 cm^{-1}; MS (EI, 70 eV) m/z (%) 508 (38), 507 (M$^+$, 100), 290 (51); HRMS (ESI) calcd for C$_{33}$H$_{38}$N$_3$O$_2$ 508.2964; found 508.2962 (M+H$^+$).

4.2.5. 3-Benzyl-5-(4-hydroxyphenyl)-6-methyl-2-octa-namidopyrazine (3bH). To a solution of 3-benzyl-5-(4-benzyloxyphenyl)-6-methyl-2-octanamidopyrazine (31 mg, 0.062 mmol) in 20 mL of ethanol/ethyl acetate (1:1) was added 12 mg of Pd/C powder. The suspension was stirred at room temperature overnight under H$_2$ and was filtered through Celite. The filtrate was concentrated in vacuo and the residue was purified by recrystallization, yielding 3-benzyl-5-(4-hydroxyphenyl)-6-methyl-2-octanamidopyrazine (**3bH**) (17 mg, 67%) as colorless cubes: mp 176.5–177 °C; ^{1}H NMR (CDCl$_3$) δ 7.41 (AA′BB′, 2H), 7.16–7.30 (m, 5H), 6.82 (AA′BB′, 2H), 6.12 (br s, 1H), 4.27 (s, 2H), 2.50 (s, 3H), 2.36 (t, J=7.8 Hz, 2H), 1.64 (quint, 2H), 1.28–1.31 (m, 8H), 0.89 (t, J=8.9 Hz, 3H); ^{13}C NMR (CDCl$_3$) δ 173.0 (s), 156.6 (s), 150.5 (s), 147.4 (s), 142.0 (s), 140.3 (s), 138.0 (s), 130.6 (d, 2C), 130.1 (s), 128.7 (d, 2C), 128.6 (d, 2C), 126.7 (d), 115.3 (d), 40.7 (t), 36.7 (t), 31.6 (t), 29.2 (t), 29.0 (t), 25.1 (t), 22.6 (q), 22.4 (t), 14.1 (q); IR (KBr) 3293, 2927, 2854, 1663, 1611, 1569, 1496, 1400 cm^{-1}; MS (EI, 70 eV)

m/z (%) 418 (30), 417 (M$^+$, 100), 291 (72), 290 (44); HRMS (EI, 70 eV) calcd for C$_{26}$H$_{31}$N$_3$O$_2$ 417.2416; found 417.2424 (M$^+$).

4.3. Formation constant K of the 1:1 hydrogen-bonded complexes of 3aH with TMG and DBU in benzene

The equilibrium to form the 1:1 hydrogen-bonded complex [BASE⋯**3aH**] is shown in Scheme 5.[17b] To estimate the K of [TMG⋯**3aH**] and [DBU⋯**3aH**] in benzene, we measured UV–vis absorption spectra of **3aH** in benzene in the absence and the presence of various concentrations of TMG and DBU, as shown in Figure 5. The concentrations of TMG and DBU were in the ranges of 2.0×10^{-5}–0.050 and 1.0×10^{-5}–0.010 mol L^{-1}, respectively.

The observed spectral changes with clear isosbestic points were analyzed by Eq. 1 below.[46] The value A_0 is absorbance of **3aH** at a chosen wavelength in the absence of BASE. After addition of BASE, absorbance at the chosen wavelength is observed as A_{obs}. The difference between A_{obs} and A_0 is given by

$$A_{obs} - A_0 = 0.5\Delta\varepsilon\Big([\mathbf{3aH}] + [BASE] + 1/K - \big\{([\mathbf{3aH}] + [BASE] + 1/K)^2 - 4[\mathbf{3aH}][BASE]\big\}^{1/2}\Big), \quad (1)$$

where [**3aH**] and [BASE] are the initial concentrations of **3aH** and BASE, respectively, and $\Delta\varepsilon$ is the difference in the molar absorptivity between **3aH** and [BASE⋯**3aH**] at the chosen wavelength. The ($A_{obs}-A_0$) values were plotted against [TMG] and [DBU], as shown in Figure 5B, D. The data were analyzed by a nonlinear least squares curve fitting Eq. 1, giving the K values 1430±40 and 7800±400 mol^{-1} L at 25 °C, respectively, accompanied by the $\Delta\varepsilon$ values 6680±40 (350 nm) and 8300±100 (355 nm) mol^{-1} L cm^{-1}, respectively.

4.4. Formation constant K of the ion pair of 3b(O)$^-$ with TMG–H$^+$ in DMSO

The formation constant K (Scheme 5) of [TMG–H$^+$/**3b(O)**$^-$] was estimated by an analysis of an absorption spectral change of **3bH** (1.5×10^{-5} mol L^{-1}) in DMSO in the absence and the presence of various concentrations of TMG (2.0×10^{-3}–0.25 mol L^{-1}), as shown in Figure 6.

The observed spectral change gave the differences between A_{obs} and A_0, which were analyzed by Eq. 2:

$$A_{obs} - A_0 = 0.5\Delta\varepsilon\Big([\mathbf{3bH}] + [TMG] + 1/K - \big\{([\mathbf{3bH}] + [TMG] + 1/K)^2 - 4[\mathbf{3aH}][TMG]\big\}^{1/2}\Big), \quad (2)$$

where [**3bH**] and [TMG] are the initial concentrations and $\Delta\varepsilon$ is the difference in the molar absorptivity between **3bH** and [TMG–H$^+$/**3b(O)**$^-$] at a chosen wavelength.[46] The ($A_{obs}-A_0$) values were plotted against [TMG], as shown in Figure 6B, and were analyzed by a nonlinear least squares
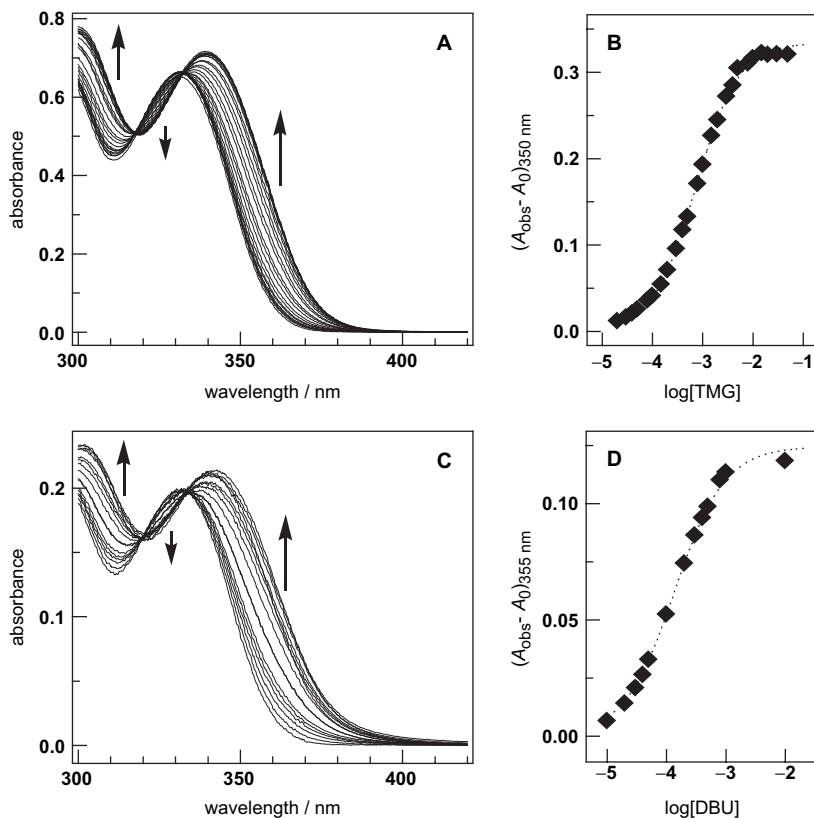
Figure 5. UV–vis absorption spectra of **3aH** in benzene containing various concentrations of TMG (A) and DBU (C) at 25 °C and plots of $(A_{obs}-A_0)$ at 350 nm versus log[TMG] (B) and $(A_{obs}-A_0)$ at 355 nm versus log[DBU] (D) for 1:1 hydrogen-bonded complexation. The initial concentrations of **3aH** were 5.0 and 1.5×10^{-5} mol L^{-1} for A and B, respectively. The concentration ranges of TMG and DBU were 2.0×10^{-5}–0.050 and 1.0×10^{-5}–0.010 mol L^{-1}, respectively. The dotted lines in B and D are the fitted curves corresponding to 1:1 complexation.

curve fitting Eq. 2, giving the K value 28 ± 3 mol^{-1} L at 25 °C, accompanied with the $\Delta \varepsilon$ value 4480 ± 160 (420 nm) mol^{-1} L cm^{-1}.

4.5. Quantum yields of the chemiluminescence reactions of 4

A small portion (10 or 20 μL) of a stock solution of **4** (2.0×10^{-3} mol L^{-1}) in methanol was put in a Pyrex cuvette

and the methanol was removed in vacuo. The cuvette containing **4** was placed in a luminometer with a photomultiplier tube and an aerated organic solvent (2.0 mL) was injected to the cuvette at 25 ± 1 °C. The chemiluminescence reactions of **4** were traced by monitoring intensity of the total emitted light. The Φ_{cl} values were determined as values relative to the Φ_{cl} value (0.013) of luminol in DMSO containing *t*-BuOK/*t*-BuOH under air.[47] The experimental errors of Φ_{cl} were within $\pm 10\%$.
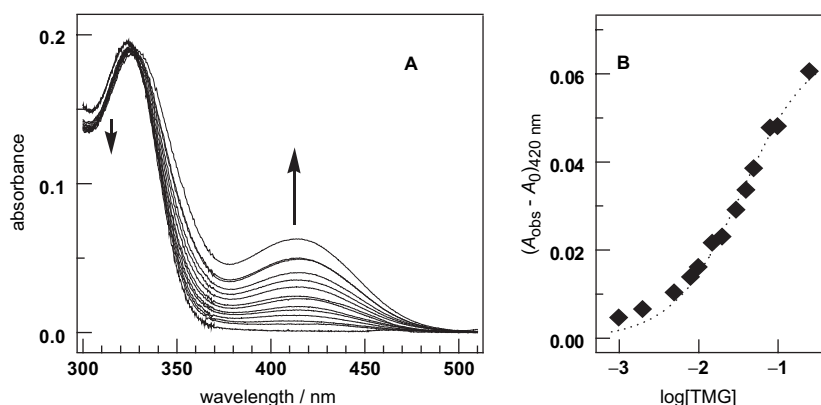

Figure 6. UV–vis absorption spectra of **3bH** (1.5×10^{-5} mol L^{-1}) in DMSO containing various concentrations of TMG (2.0×10^{-3}–0.25 mol L^{-1}) at 25 °C (A) and plot of $(A_{obs}-A_0)$ at 420 nm versus log[TMG] for ion pair generation (B). The dotted line in B is the fitted curve for ion pair generation.

References and notes

1. (a) Morin, J. G.; Hastings, J. W. *J. Cell. Physiol.* **1971**, *77*, 305–311; (b) Morin, J. G. *Coelenterate Biology: Reviews and New Perspectives*; Academic: New York, NY, 1975; pp 397–438; (c) Tsuji, F. I.; Ohmiya, Y.; Fagan, T. F.; Toh, H.; Iouye, S. *Photochem. Photobiol.* **1995**, *62*, 657–661.
2. (a) Shimomura, O.; Johnson, F. H.; Saiga, Y. *J. Cell. Comp. Physiol.* **1962**, *59*, 223–240; (b) Shimomura, O.; Johnson, F. H. *Nature* **1975**, *256*, 236–238.
3. Reviews: (a) Johnson, F. H.; Shimomura, O. *Methods Enzymol.* **1978**, *57*, 271–291; (b) Ohmiya, Y.; Hirano, T. *Chem. Biol.* **1996**, *3*, 337–347.
4. Illarionov, B. A.; Frank, L. A.; Illarionova, V. A.; Bondar, V. S.; Vysotski, E. S.; Blinks, J. R. *Methods Enzymol.* **2000**, *305*, 223–249.
5. FLP obtained from the wild type aequorin is generally called a blue fluorescent protein (BFP).[2,3]
6. Head, J. H.; Inouye, S.; Teranishi, K.; Shimomura, O. *Nature* **2000**, *405*, 372–376.
7. (a) Liu, Z.-J.; Vysotski, E. S.; Chen, C.-J.; Rose, J.; Lee, J.; Wang, B.-C. *Protein Sci.* **2000**, *9*, 2085–2093; (b) Deng, L.; Markova, S. V.; Vysotski, E. S.; Liu, Z.-J.; Lee, J.; Rose, J.; Wang, B.-C. *J. Biol. Chem.* **2004**, *279*, 33647–33652; (c) Deng, L.; Vysotski, E. S.; Markova, S. V.; Liu, Z.-J.; Lee, J.; Rose, J.; Wang, B.-C. *Protein Sci.* **2005**, *14*, 663–675; (d) Liu, Z.-J.; Stepanyuk, G. A.; Vysotski, E. S.; Lee, J.; Markova, S. V.; Malikova, N. P.; Wang, B.-C. *Proc. Natl. Acad. Sci. U.S.A.* **2006**, *103*, 2570–2575.
8. McCapra, F.; Chang, Y. C. *J. Chem. Soc., Chem. Commun.* **1967**, 1011–1012.
9. Goto, T.; Inoue, S.; Sugiura, S. *Tetrahedron Lett.* **1968**, 3873–3876.
10. Shimomura, O.; Johnson, F. H. *Biochem. Biophys. Res. Commun.* **1971**, *44*, 340–346.
11. (a) Shimomura, O.; Johnson, F. H. *Nature* **1970**, *227*, 1356–1357; (b) Shimomura, O.; Johnson, F. H. *Tetrahedron Lett.* **1973**, 2963–2966.
12. Hori, K.; Wampler, J. E.; Cormier, M. J. *J. Chem. Soc., Chem. Commun.* **1973**, 492–493.
13. McCapra, F.; Manning, M. J. *J. Chem. Soc., Chem. Commun.* **1973**, 467–468.
14. Shimomura, O. *Biochem. J.* **1995**, *306*, 537–543.
15. Hirano, T.; Mizoguchi, I.; Yamaguchi, M.; Chen, F. Q.; Ohashi, M.; Ohmiya, Y.; Tsuji, F. I. *J. Chem. Soc., Chem. Commun.* **1995**, 165–167.
16. Saito, R.; Hirano, T.; Niwa, H.; Ohashi, M. *J. Chem. Soc., Perkin Trans. 2* **1997**, 1711–1716.
17. (a) Hirano, T.; Ohmiya, Y.; Maki, S.; Niwa, H.; Ohashi, M. *Tetrahedron Lett.* **1998**, *39*, 5541–5544; (b) Imai, Y.; Shibata, T.; Maki, S.; Niwa, H.; Ohashi, M.; Hirano, T. *J. Photochem. Photobiol., A* **2001**, *146*, 95–107.
18. Pines, E. *The Chemistry of Phenol*; Rappoport, Z., Ed.; Wiley: Chichester, UK, 2003; pp 401–527.
19. Homer, R. B.; Johnson, C. D. *The Chemistry of Amide*; Zabicky, J., Ed.; Interscience: London, 1970; pp 187–243.
20. Fujimori, K.; Nakajima, H.; Akutsu, K.; Mitani, M.; Sawada, H.; Nakayama, M. *J. Chem. Soc., Perkin Trans. 2* **1993**, 2405–2409.
21. Saito, R.; Iwasa, E.; Katoh, A. *Proceedings of the 13th International Symposium on Bioluminescence & Chemiluminescence Progress and Perspectives*; Tsuji, A., Matsumoto, M., Maeda, M., Kricka, L. J., Stanley, P. E., Eds.; World Scientific: Singapore, 2005; pp 125–128.
22. (a) Vysotski, E. S.; Liu, Z.-J.; Markova, S. V.; Blinks, J. R.; Deng, L.; Frank, L. A.; Herko, M.; Malikova, N. P.; Rose, J. P.; Wang, B.-C.; Lee, J. *Biochemistry* **2003**, *42*, 6013–6024; (b) Malikova, N. P.; Stepanyuk, G. A.; Frank, L. A.; Markova, S. V.; Vysotski, E. S.; Lee, J. *FEBS Lett.* **2003**, *554*, 184–188; (c) Vysotski, E. S.; Lee, J. *Acc. Chem. Res.* **2004**, *37*, 405–415.
23. Shimomura, O.; Teranishi, K. *Luminescence* **2000**, *15*, 51–58.
24. (a) Shimomura, O.; Musicki, B.; Kishi, Y. *Biochem. J.* **1989**, *261*, 913–920; (b) Shimomura, O.; Musicki, B.; Kishi, Y.; Inouye, S. *Cell Calcium* **1993**, *14*, 373–378.
25. Reichardt, C. *Solvents and Solvent Effects in Organic Chemistry*, 3rd ed.; Wiley-VCH: Weinheim, 2003.
26. Kolthoff, I. M.; Chantooni, M. K., Jr.; Bhowmik, S. *J. Am. Chem. Soc.* **1968**, *90*, 23–28.
27. While we previously correlated the E_{FL} of **3a(O)**$^-$ in the ion pairs with NBA–H$^+$ and TMG–H$^+$ to $E_T(30)$ for making one plot,[17b] we had to revise the previous one to the E_{FL}–$E_T(30)$ correlations in the text.
28. The λ_{FL} and Φ_f values of **3aH** and/or **3a(O)**$^-$ were partially reported in the previous report.[17b] The previous data were collected with a spectrometer older than that used in this report. We carefully reinvestigated the fluorescence behaviors of **3aH** and **3a(O)**$^-$ in this work. Then, we revised the λ_{FL} and Φ_f values reported previously.
29. *Ions and Ion Pairs in Organic Reactions*; Szwarc, M., Ed.; Wiley-Interscience: New York, NY, 1972; Vol. 1.
30. Brown, H. C.; Okamoto, Y. *J. Am. Chem. Soc.* **1958**, *80*, 4979–4987.
31. Hansch, C.; Leo, A.; Taft, R. W. *Chem. Rev.* **1991**, *91*, 165–195.
32. (a) Hirano, T.; Gomi, Y.; Takahashi, T.; Kitahara, K.; Chen, F. Q.; Mizoguchi, I.; Kyushin, S.; Ohashi, M. *Tetrahedron Lett.* **1992**, *33*, 5771–5774; (b) Saito, R.; Hirano, T.; Niwa, H.; Ohashi, M. *Chem. Lett.* **1998**, 95–96.
33. Usami, K.; Isobe, M. *Tetrahedron* **1996**, *52*, 12061–12090.
34. Teranishi, K.; Hisamitsu, M.; Yamada, T. *Tetrahedron Lett.* **1997**, *38*, 2689–2692.
35. Kondo, H.; Igarashi, T.; Maki, S.; Niwa, H.; Ikeda, H.; Hirano, T. *Tetrahedron Lett.* **2005**, *46*, 7701–7704.
36. Klamt, A.; Schuurmann, G. *J. Chem. Soc., Perkin Trans. 2* **1993**, 799–805.
37. Shimomura, O.; Johnson, F. H. *Biochemistry* **1969**, *8*, 3991–3997.
38. Markova, S. V.; Vysotski, E. S.; Blinks, J. R.; Burakova, L. P.; Wang, B.-C.; Lee, J. *Biochemistry* **2002**, *41*, 2227–2236.

39. Toma, S.; Chong, K. T.; Nakagawa, A.; Teranishi, K.; Iouye, S.; Shimomura, O. *Protein Sci.* **2005**, *14*, 409–416.

40. Streitwieser, A.; Kim, Y.-J. *J. Am. Chem. Soc.* **2000**, *122*, 11783–11786.

41. Very recently, a reaction mechanism similar to ours was proposed based on evaluating the active site structure of FLP of obelin.[7d] Our mechanism contains the chemiexcitation process from dioxetanone intermediate **11**⁻ possessing a 4-oxidophenyl group to ¹**2(O)**⁻*, while their mechanism contains the chemiexcitation process from a neutral dioxetanone intermediate to neutral excited molecule ¹**2H***. Thus, there is an important difference in the chemiexcitation processes between the two mechanisms.

42. The authors thank one of the referees for his/her valuable comment on the other bioluminescence using coelenterazine as a luciferin. At present our molecular mechanism for calcium-activated photoproteins (Scheme 10) is not applicable to the bioluminescence of a deep-sea shrimp *Oplophorus*, because bisdeoxycoelenterazine, an analogue of coelenterazine, has a bioluminescent activity for the reactions using *Oplophorus* luciferase: Nakamura, H.; Wu, C.; Murai, A.; Inouye, S.; Shimomura, O. *Tetrahedron Lett.* **1997**, *38*, 6405–6406.

43. Stewart, J. J. P. *MOPAC 2002*; Fujitsu: Tokyo, Japan, 2001.

44. Inoue, S.; Sugiura, S.; Kakoi, H.; Goto, T. *Tetrahedron Lett.* **1969**, 1609–1610.

45. Sharefkin, D. M. *J. Am. Chem. Soc.* **1959**, *24*, 345–348.

46. Schneider, H. J.; Yatsimirsky, A. *Principles and Methods in Supramolecular Chemistry*; Wiley: Chichester, UK, 2000.

47. Lee, J.; Seliger, H. H. *Photochem. Photobiol.* **1972**, *15*, 227–237.